4-1-1994

BASIC RESONANT TOPOLOGIES FOR SWITCHING POWER SUPPLIES

Zacharias K. Vachaparambil
Purdue University School of Electrical Engineering

BASIC RESONANT TOPOLOGIES FOR SWITCHING POWER SUPPLIES

ZACHARIAS K. VACHAPARAMBIL

TR-EE 94-12
APRIL 1994

SCHOOL OF ELECTRICAL ENGINEERING
PURDUE UNIVERSITY
WEST LAFAYETTE, INDIANA 47907-1285

BASIC RESONANT TOPOLOGIES FOR SWITCHING POWER SUPPLIES

Zacharias K. Vachaparambil

Purdue Electric Power Center
School of Electrical Engineering
Purdue University
1285 Electrical Engineering Building
West Lafayette, IN 47907-1285

TABLE OF CNTENTS

Page

LIST OF FIGURES

Figure Page

Appendix
Figure

NOMENCLATURE

SRC = series resonant converter

PRC = parallel resonant converter

DC = direct current

AC = alternating current,

MOSFET= metal oxide semiconductor field effect transistor

PWM = pulse width modulation

FM = frequency modulation

SPRC = series parallel resonant converter

CCM = continous conduction mode

DCM = discontinous concluction mode

CCVM = clamped capacitor voltage mode

ABSTRACT

The objective of this thesis is to study the basic resonant converter topologies for switching power supplies and to compare their performance under different operating conditions. The series and parallel resonant converters are analyzed in detail. The analysis uses the state plane method, which gives a good insight of the operation of the converter. It is found that these converters have more desirable characteristics when operated at a frequency above the resonant frequency rather than below it. Analytical results are verified by simulation and experiment.

1. INTRODUCTION

1.1 Background

During recent years, resonant converters have gained renewed interest due to their advantages of higher efficiency, smaller size and weight for passive components and lesser EMI problems over the conventional PWM switching converters. Though they had been present for a long time, their applications were limited until the advent of high speed, low cost, controllable, power semiconductor switches. Nowadays, resonant converters arc widely used for switching power supplies, AC motor drives and various other applications. It is widely perceived as the best candidate for the next generation of power converters.

To bring out the advantages of resonant mode power conversion, some of the problems associated with conventional hard switched PWM converters will be cliscussed first.

1. The switches are required to turn on or turn off the entire load current during each state transition. Thus the switches are subjected to high switching stresses and results in significant switching losses in the converter. Since switching losses increases linearly with the switching frequency, it constitutes the major portion of the losses in a high frequency PWM converter.

2. When switching losses imposes an upper bound on the switching frequency that can be used, a further reduction in the size and weight of the transformer or the filter components is not possible.

3. The switches are required to have high di/dt and dv/dt capabilities to make the switching transitions fast so that switching losses are kept at a minimum. But

these fast transitions in voltage and current produce electromagnetic interference.

Tlie basic strategy of resonant converters is to eliminate or reduce significantly the switching losses in the converter. This is achieved by making either the current through the switch or the voltage across it zero at the time when the switch changes state. Switching stresses as well as EMI problems arc also reduced so that very high switching frequencies are possible. Resonant converters achieve the above advantages at tlie penalty of higher on-state currents and off-state voltages for the power switches. Also the methods of control are more complex compared to that of PWM converters.

Resonant converters can he broadly classified as

1. Load resonant converters. These are referred to as simply resonant converters. Here the load is a part of the resonant circuit so that either it carries the resonant current or the resonant capacitor's voltage appears across it. The power flow to tlie load is controlled by the converter switching frequency in comparison to the resonant frequency of the LC' tank.

2. Quasi-resonant converters. These arc also called resonant switch converters. Here LC resonance is used only to shape the switch voltage and current to provide either a zero-voltage or a zero-current switching.

3. Resonant DC-link converters. These are typically used in conjunction with DC-**AC** inverters in AC drives. Here, LC resonance is utilized to make the DC voltage oscillate around some DC value so that it has a zero crossing during which the status of the inverter switches can he changed.

1.2 Purpose of Study

In this thesis we will be studying only load resonant converters. As mentioned he-fore, resonant converters are widely used in high frequency switching power supplies. Although operation of converters below resonance had been well studied [LK86] their

operation above resonance has attracted much less attention. This thesis also makes a comparative study of the operation of basic resonant topologies above and below resonance. The feasibility of operating the converter above resonance is investigated.

The state plane method is employed as the basic analysis tool. While time domain rncthods are equally applicable, state plane diagram gives a better insight of the converter operation. It can clearly portray the steady state as well as transient operation of resonant converters. The anomalous sequences of conduction often encountered in practical systems can he well explained with the state plane diagram. Since the state plane directly indicates the resonant tank energy level at which the system is operating, the ability of a controller to keep tank energy level within bounds under transient contlitions can be easily evaluated with this method.

It must be notetl that there are several nonconventional topologies achieving specific advantages. Most of them need special treatnient from an analysis point of view. Here instead, an analysis of the generic converter topologies is done which can be extended to various derived topologies.

1.3 Outline of Thesis

This thesis contains five chapters. In Chapter 2, operation of the series resonant, converter above and below resonance is analyzed in detail. Simulation as well as experimental results are provided for frequency of operation above resonance.

Chapter 3 discusses the parallel resonant converter, which is a more popular resonant topology. Chapter 4 gives a short account of the series parallel resonant converter which is actually a modification of the parallel resonant converter. It combines the advantages of both series and parallel resonant, converters while eliminating many of their disadvantages. Hence it is regarded as an optimum converter topology. A discussion of the control of resonant converters is also included at the end of the chapter.

Chapter 5 summarizes the conclusions obtained from this study.

2. SERIES RESONANT CONVERTER

2.1 Circuit Operation

A conventional lialf-bridge series resonant converter(SRC) circuit is shown in Fig. 2.1. The parallel combination of a transistor and a diode form a bidirectional switch which operates at a fifty percent duty ratio to generate a symmetrical square wave voltage across the resonant circuit. The resonant current is coupled to the output circuit through the full wave rectifier. The output capacitor C_0 serves as a constant voltage sink under steady state and is chosen to be much larger than the resonant capacitor C. A transformer can be included for a desired output voltage as well as input-output isolation. In the following analysis it is assumed that the converter is operating in the continuous conduction mode.

2.2 Operation Above Resonance

In this mode of operation the power switches turn off at a finite current but they turn on at, zero current and zero voltage. The diodes turn off naturally. Hence there are turn off losses only for the power switches. The following assumptions are made in the analysis.

1. There are no losses in the converter. The tank circuit is assumed to have infinite quality factor Q.
2. All switches have zero resistance when on.
3. All diodes have zero forward resistance and infinite reverse resistance.
4. The output filter time constant is much longer than the time constant of the resonant circuit. Thus the output voltage may be considered constant.

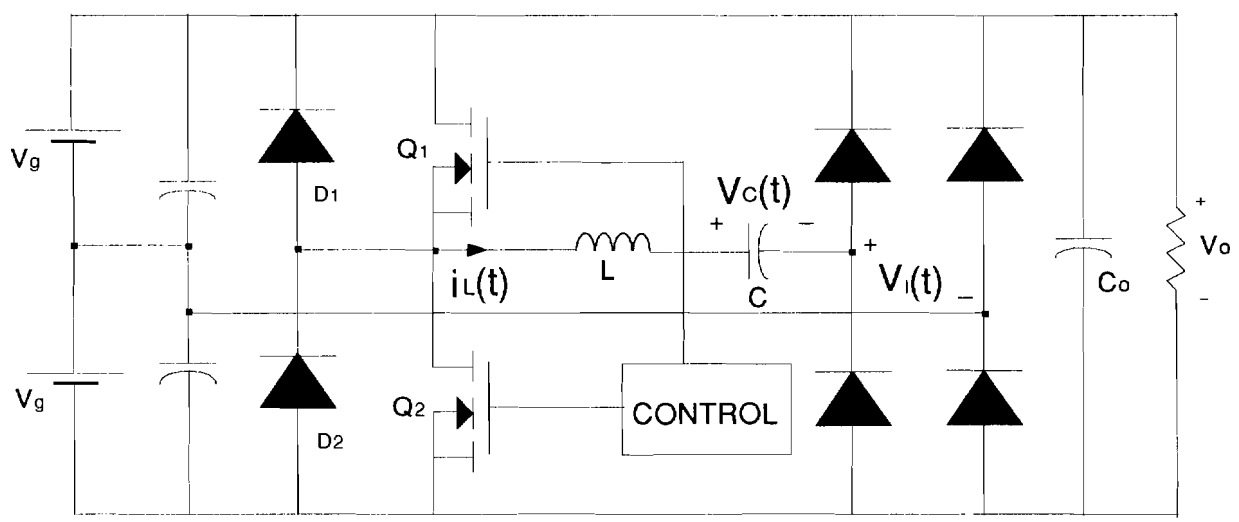

Figure 2.1 Conventional SRC circuit diagram

5. The switches turn off instantaneously.

6. Only fundamental waveforms are used in the analysis.

The operation of the converter over one switching period can be divided into four intervals based on the device being conclucting, i.e., Q_1, D_2, Q_2 or D_1. In the following section these circuit modes and the governing equations will be derived.

Mode 1 ($t_0 \leq t \leq t_1$)

Assume Q_1 is turned on at this time. Then D_1, Q_2 and D_2 are off. The circuit can be reduced as the one shown in Fig. 2.2 (a). The governing equations of this circuit mode arc given by

$$\frac{di_l(t)}{dt} = \frac{V_g - v_c(t) - V_0}{L} \quad [2.1]$$

$$\frac{dv_c(t)}{dt} = \frac{1}{C} i_l(t) \quad [2.2]$$

Since it is much easier lo work with normalized quantities, we will use the following normalization factors.

$$V_{base} = V_g \quad I_{base} = V_g/Z_0 \quad f_{base} = f_0 = 1/2\pi\sqrt{LC}$$

where $Z_0 = \sqrt{L/C}$ is the characteristic impedance of the resonant circuit and f_0 is the resonant frequency. Using these normalized quantities in the above equations,

$$\frac{di_{nl}(t)}{dt} = \omega_0 \, (1 - v_{nc}(t) - V_{n0}) \quad [2.3]$$

$$\frac{dv_{nc}(t)}{dt} = \omega_0 \, i_{nl}(t) \quad [2.4]$$

where ω_0 is the resonant frequency in rad/sec. By combining 2.3 and 2.4 we get

$$\frac{di_{nl}}{dv_{nc}} = \frac{(1 - v_{nc} - V_{n0})}{i_{nl}} \quad [2.5]$$

Mode 2 ($t_1 \leq t \leq t_2$)

In this mode switch Q_1 is forced to turn off at t_1. Since the resonant current $i_{nl}(t)$ is

positive it flows through D_2 while Q_1,Q_2 and D_1 are off. The equivalent circuit for this mode is shown in Fig. 2.2 (b). The corresponding normalized equations arc

$$\frac{di_{nl}(t)}{dt} = \omega_0 \left(-1 - v_{nc}(t) - V_{n0}\right) \quad [2.6]$$

$$\frac{dv_{nc}(t)}{dt} = \omega_0 \, i_{nl}(t) \quad [2.7]$$

By combining 2.6 and 2.7 we get

$$\frac{di_{nl}}{dv_{nc}} = \frac{(-1 - v_{nc} - V_{n0})}{i_{nl}} \quad [2.8]$$

Mode 3 ($t_2 \leq t \leq t_3$)

At time t_2, D_2 is turned off naturally since the inductor current becomes zero. Now Q_2 turns on at zero voltage since it is gated as soon as D_2 starts conducting. D_1,Q_1,and D_2 arc held off. The circuit can be reduced as the M_3 mode circuit shown in Fig. 2.2(c). The corresponding normalized equations are

$$\frac{di_{nl}(t)}{dt} = \omega_0 \left(-1 - v_{nc}(t) + V_{n0}\right) \quad [2.9]$$

$$\frac{dv_{nc}(t)}{dt} = \omega_0 \, i_{nl}(t) \quad [2.10]$$

By combining 2.9 and 2.10 we get

$$\frac{di_{nl}}{dv_{nc}} = \frac{(-1 - v_{nc} + V_{n0})}{i_{nl}} \quad [2.11]$$

Mode 4 (t_3 I t / $t4$)

At time t_3, Q_2 is force commutated. Since the inductor current is negative, it is forced to flow through D_1. While D_1 is conducting D_2,Q_1,and Q_2 are off. The circuit can be reduced as the M_4 mode circuit shown in Fig. 2.2 (d). The corresponding normalized equations are

$$\frac{di_{nl}(t)}{dt} = \omega_0 \left(1 - v_{nc}(t) + V_{n0}\right) \quad [2.12]$$

$$\frac{dv_{nc}(t)}{dt} = \omega_0 \, i_{nl}(t) \quad [2.13]$$

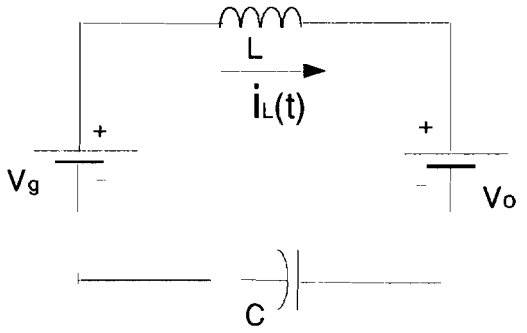

(a) Mode 1

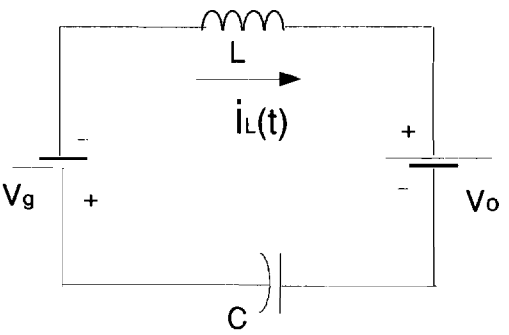

(b) Mode 2

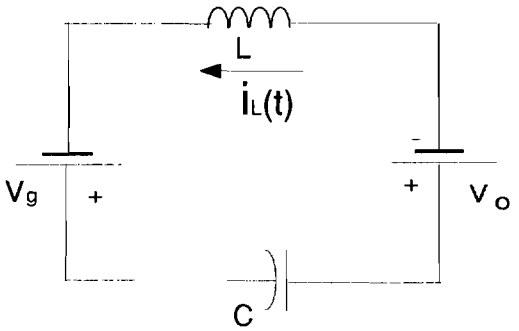

(c) Mode 3

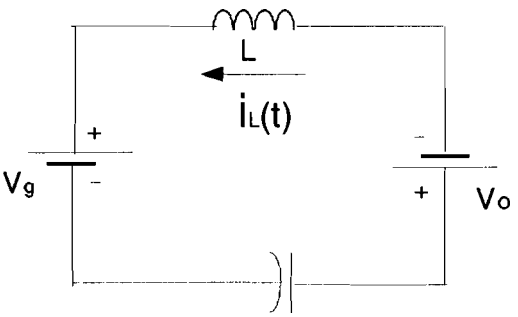

(d) Mode 4

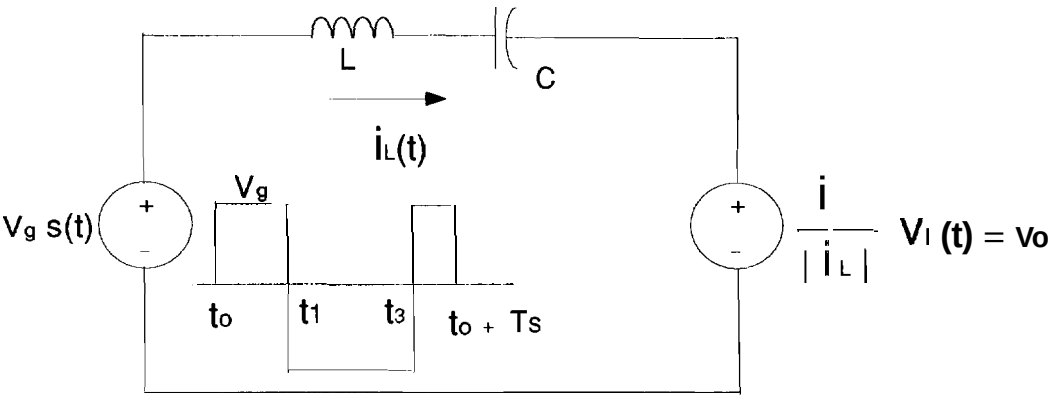

(e) SRC equivalent circuit

Figure 2.2 Four modes in the operation of SRC

By combining 2.12 and 2.13 we get

$$\frac{di_{nl}}{dv_{nc}} = \frac{(1 - v_{nc} + V_{n0})}{i_{nl}} \qquad [2.14]$$

This process repeats for each switching period. For the steady state analysis of the converter the equivalent circuit shown in Fig. 2.2 (c) can be used. The driving source is $V_g s(t)$ and the voltage sink is $V_l(t)$ where $s(t)$ is a 50% duty cycle square wave of amplitude unity and period equal to T_s. $V_l(t)$ whose sign is determined by the direction of the resonant current $i_l(t)$ has the value of the output voltage V_0. Typical steady slate voltage and current waveforms for the tank circuit are shown in Fig. 2.3.

2.2.1 State Plane Analysis

The steady state response of SRC can be described by means of the v–i trajectory in the state plane. If the resonant circuit is lossless, the v–i trajectory is a closecl contour consisting of sections of circular arcs. The centers of these circular arcs are tlie singular points or equilibrium points of the differential equations describing the particular mode. At the singular points

$$\frac{di_{nl}(t)}{dt} = 0 \quad \text{and} \quad \frac{dv_{nc}(t)}{dt} = 0$$

and the solution of 2.3 and 2.4 is not unique.

Integrating both sides of 2.5,

$$i_{nl}^2 + (v_{nc} - (1 - V_{n0}))^2 = k^2 \qquad [2.15]$$

where k^2 is a constant which can be obtained by evaluating 2.15 at $t = t_0$. Thus

$$\begin{aligned} k^2 &= (-V_{ncmax} - (1 - V_{n0}))^2 \\ &= (V_{ncmax} + 1 - V_{n0})^2 \end{aligned} \qquad [2.16]$$

Similarly by solving 2.8, 2.11 and 2.14 a set of normalized state plane equations describing the complete v-i trajectory over one switching period can be obtained.

$$i_{nl}^2 + (v_{nc} - (1 - V_{n0}))^2 = V_{nM1}^2 \qquad t_0 \le t \le t_1 \qquad [2.17]$$

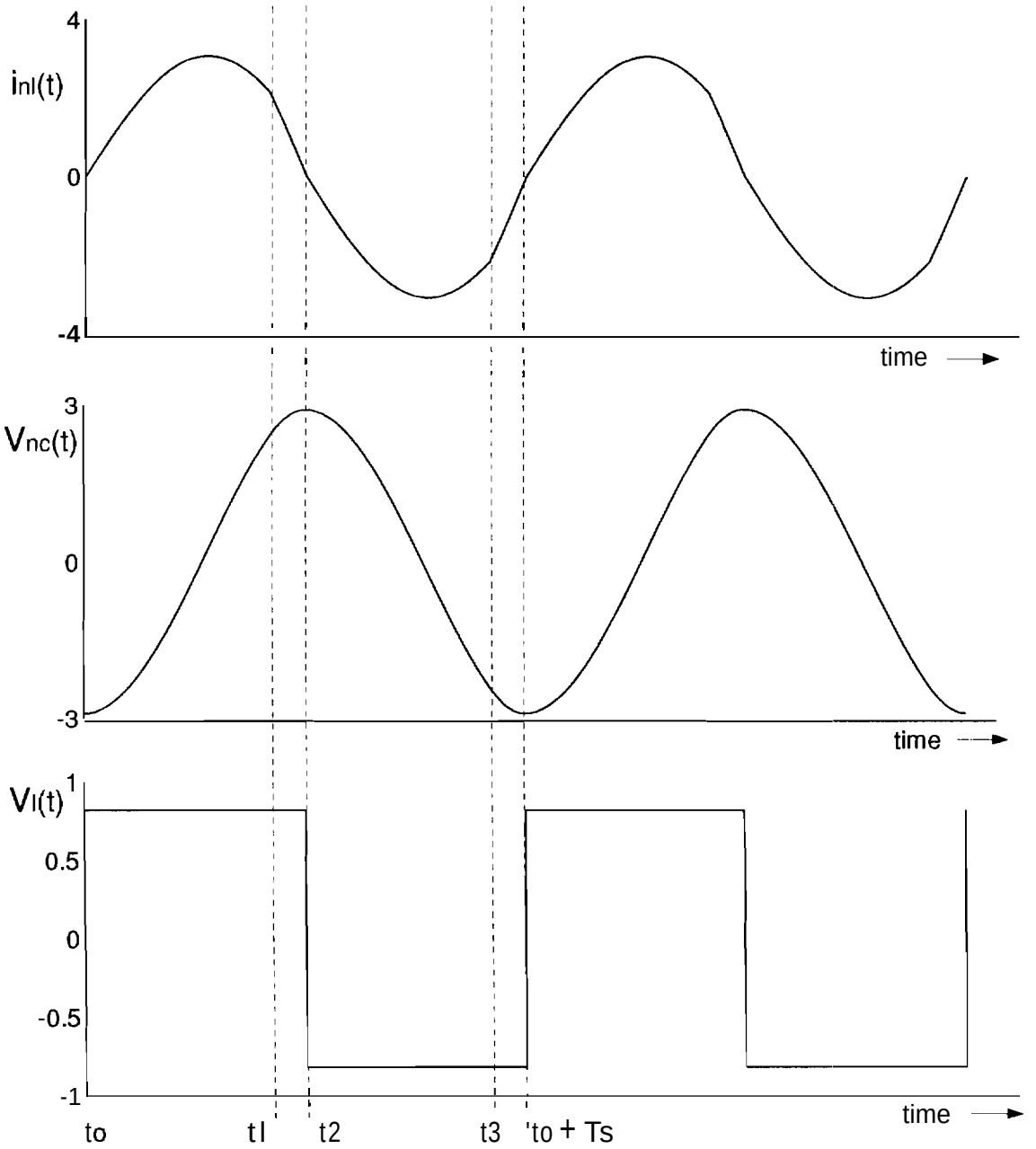

Figure 2.3 Steady state waveforms in continuous conduction mode

$$i_{nl}^2 + (v_{nc} - (-1 - V_{n0}))^2 = V_{nM2}^2 \qquad t_1 \le t \le t_0 + T_s/2 \qquad [2.18]$$

$$i_{nl}^2 + (v_{nc} - (-1 + V_{n0}))^2 = V_{nM3}^2 \qquad t_0 + T_s/2 \le t \le t_3 \qquad [2.19]$$

$$i_{nl}^2 + (v_{nc} - (1 + V_{n0}))^2 = V_{nM4}^2 \qquad t_3 \le t \le t_0 + T_s \qquad [2.20]$$

where

$$V_{nM1} = V_{nM3} = V_{ncmax} + 1 - V_{n0} \qquad [2.21]$$

$$V_{nM2} = V_{nM4} = V_{ncmax} + 1 + V_{n0} \qquad [2.22]$$

and V_{ncmax} is the normalized absolute value of the resonant capacitor voltage at. zero resonant current. Equations 2.17 through 2.18 can he represented by a state plane diagram and il is shown in Fig. 2.3. The conduction angle of diode D_1 and D_2 is α while that of Q_1 and Q_2 is β. The singular point for each circuit mode can he obtained from equations 2.17 through 2.18 as

$$M_1 : [(1 - V_{n0}), 0]$$
$$M_2 : [(-1 - V_{n0}), 0]$$
$$M_3 : [(-1 + V_{n0}), 0]$$
$$M_4 : [(1 + V_{n0}), 0]$$

The state transition of the SRC is in the arrow direction shown in Fig. 2.4 as time proceeds. The sum of α and β, defined as the parameter γ, can be used to describe the ratio of the resonant frequency f_0 to the switching frequency f_s of the converter,that

$$\gamma = \alpha + \beta = \omega_0 \frac{T_s}{2} = \frac{\pi}{f_s/f_0} \qquad [2.23]$$

From the stale plane diagram shown in Fig. 2.4 it is easy to see that

$$V_{nM2} = V_{nM1} + 2V_{n0} \qquad [2.24]$$

and from $\triangle$ PQR

$$V_{nM1}^2 + V_{nM2}^2 + 2V_{nM1}V_{nM2}\cos(\gamma) = 4 \qquad [2.25]$$

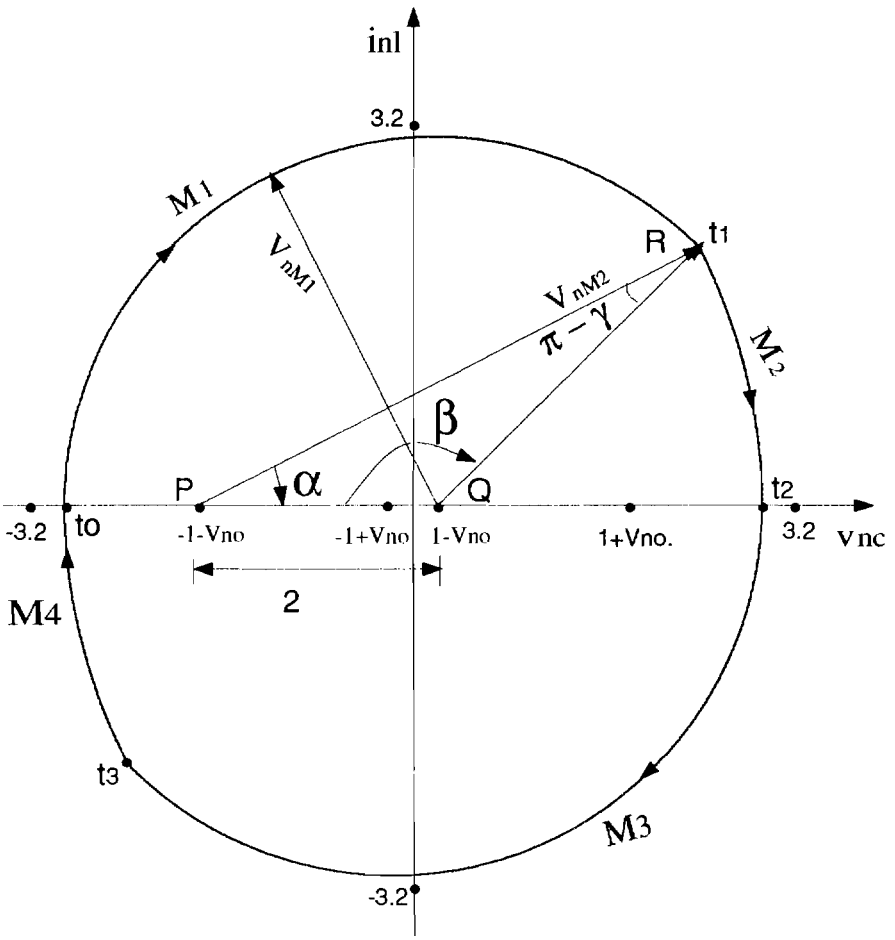

Figure 2.4 SRC state plane diagram for $f_s > f_0$

By solving 2.24 and 2.25, V_{nM1} can be obtained in terms of voltage gain V_{n0} and switching frequency ratio y

$$V_{nM1} = \sqrt{\frac{1 - V_{n0}^2 \sin^2(\gamma/2)}{cos^2(\gamma/2)}} - V_{n0} \qquad [2.26]$$

Then V_{nM2} can be obtained from equation 2.24. In order lo find the switching boundary we can substitute $t = t_1$ into 2.17 and 2.18 which yields

$$i_{nl}^2(t_1) + [v_{nc}(t_1) - (1 - V_{n0})]^2 = V_{nM1}^2 \qquad [2.27]$$

$$i_{nl}^2(t_1) + [v_{nc}(t_1) + (1 + V_{n0})]^2 = V_{nM2}^2 \qquad [2.28]$$

The switching boundary then can be obtained by solving 2.27 and 2.28. The solutions are given by

$$|v_{nc}(t_1)| = V_{n0}\,(V_{nM1} - 1 + V_{n0}) \qquad [2.29]$$

$$|i_{nl}(t_1)| = \sqrt{(1 - V_{n0}^2)[(V_{nM1} + V_{n0})^2 - 1]} \qquad [2.30]$$

Once the above information is obtained we can move into the next section to deri ve the control characteristics.

2.2.2 Control Characteristics

The control characteristics of the converter are very important in converter design. If any two of the variables among converter gain M (which is the same as V_{n0}), switching frequency ratio γ and output load Q are specified. the third variable can be determined. From this the variation in voltage gain and switching frequency due to load changes can be easily inferred. The normalized output DC current I_{n0} can be found as

$$\begin{aligned} I_{n0} &= 2(I_{nQ} + I_{nD}) \\ &= \frac{2}{T_s}\left(\int_{t_0}^{t_1} i_{nl}(t)\,dt + \int_{t_1}^{t_0+T_s/2} i_{nl}(t)\,dt\right) \\ &= \frac{2V_{ncmax}}{\gamma} \end{aligned} \qquad [2.31]$$

where I_{nQ} and I_{nD} are the normalized average currents in one switching transistor and one of the output diodes respectively. The output DC voltage is related to the output DC current I)?-

$$V_0 = R_0 I_0 \quad [2.32]$$

The above equation upon normalizing becomes

$$V_{n0} = I_{n0}/Q \quad [2.33]$$

where $Q = Z_0/\mathrm{R}$. Thus the voltage gain and the normalized average output power which is $V_{n0} I_{n0}$ can be expressed as

$$M = \frac{2V_{ncmax}}{\gamma Q} \quad [2.34]$$

$$P_{n0} = \frac{4V_{ncmax}^2}{\gamma^2 Q} \quad [2.35]$$

where

$$V_{ncmax} = -1 + M + V_{nM1} \quad [2.36]$$

Thus equation 2.34 can be written as

$$Q = \frac{2(-1 + M + V_{nM1})}{\gamma M} \quad [2.37]$$

Substituting for V_{nM1} from 2.26 and after a few steps of manipulation we obtain

$$aM^2 + bM + c = 0 \quad [2.38]$$

where

$$a = \gamma^2 Q^2 \cos^2(\gamma/2) + 4\sin^2(\gamma/2)$$

$$b = 4\gamma Q \cos^2(\gamma/2)$$

$$c = 4(\cos^2(\gamma/2) - 1)$$

By solving for M in equation 2.38 the control characteristics of the converter can he obtained and is plol ted in Fig. 2.5 for different output load Q. From the characteristics it can be seen that for high values of the switching frequency the converter gain is rather independent of the load.

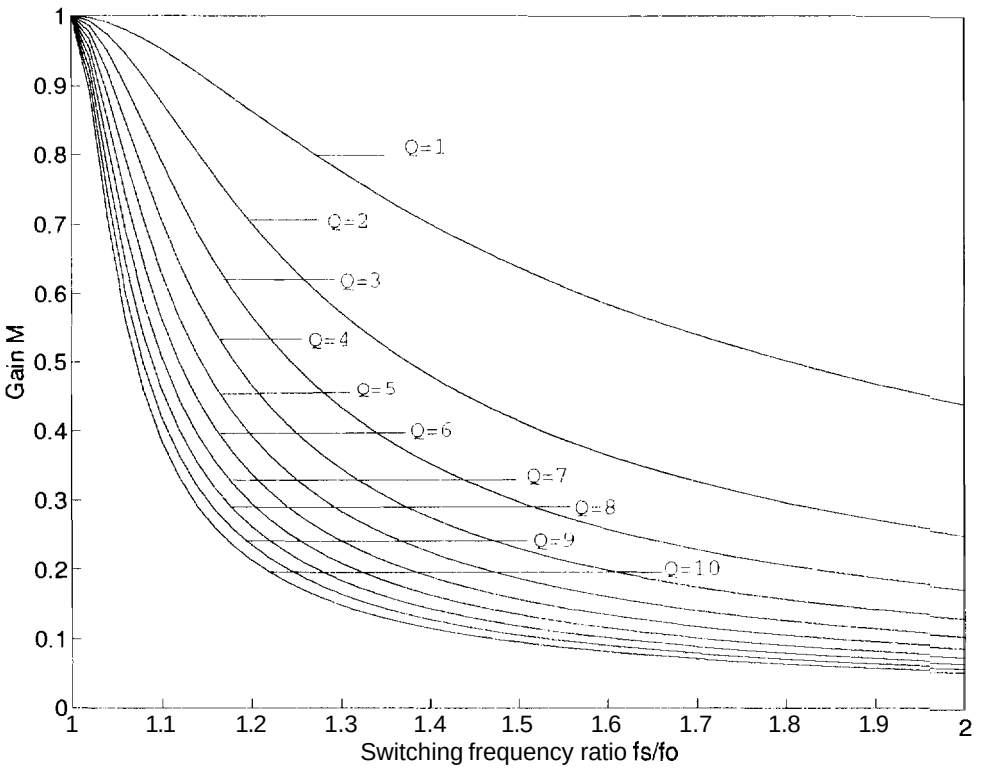

Figure 2.5 SRC control characteristic curves for $f_s > f_0$

2.2.3 Component Stresses

Based on the state plane diagram and the operating conditions of the converter the coinponent stresses can be derived analytically. The normalized average switch current can be calculated as

$$I_{nQ} = \frac{1}{2\gamma}\int_0^{\beta} V_{nM1} sin(\omega_0 t)\, d(\omega_0 t) \qquad [2.39]$$

which when evaluated and simplified reduces to

$$I_{nQ} = \frac{V_{ncmax}}{2\gamma}(1+M) \qquad [2.40]$$

Similarly the normalized average current in each diode is

$$I_{nD} = \frac{1}{2\gamma}\int_{\beta}^{\alpha+\beta} V_{nM2} sin(\gamma - \omega_0 t) d(\omega_0 t) \qquad [2.41]$$

$$= \frac{V_{ncmax}}{2\gamma}(1-M) \qquad [2.42]$$

The peak resonant capacitor voltage can be obtained from equation 2.21 as

$$V_{ncmax} = V_{nM1} - 1 + V_{no} \qquad [2.43]$$

Note that from Fig. 2.4 the peak inductor current is

$$i_{nlmax} = \begin{cases} V_{nM1} & \text{if } v_{nc}(t_1) \geq (1 - V_{n0}) \\ i_{nl}(t_1) & \text{otherwise} \end{cases} \qquad [2.44]$$

Hence from equations 2.26 and 2.30 we can obtain an expression for the normalized peak inductor current,.

These quantities arc plotted in Fig. 2.6 as a function of the switching frequency for different values of the converter gain.

2.2.4 Design of Converter

In this section a simple method for designing a series resonant converter will be illustrated. If we specify any two of the parameters among M, Q, I_{n0} and γ a complete

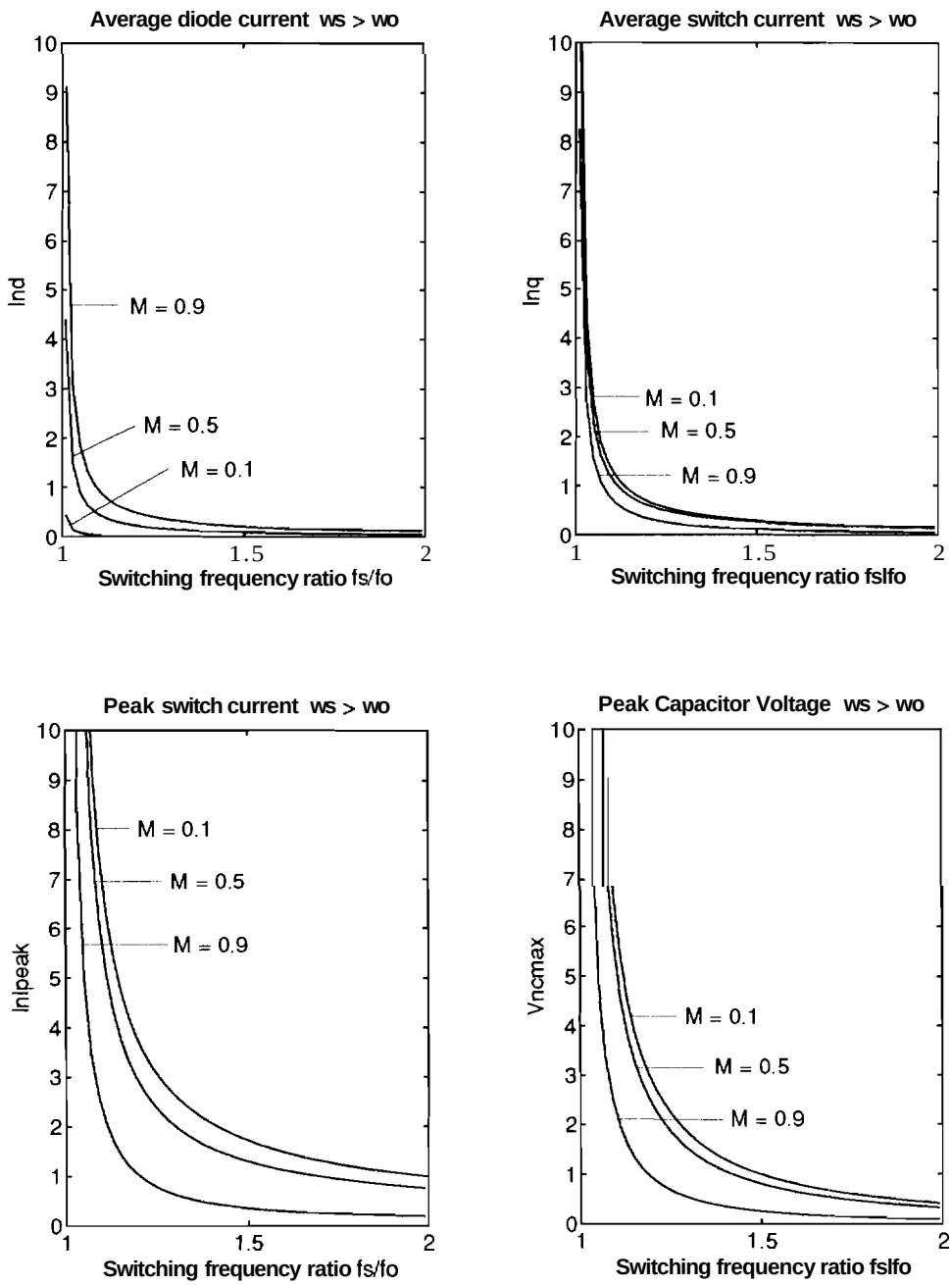

Figure 2.6 Component stresses as a function of switching frequency

design can be obtained. We will design a converter with the following specifications.

Main input DC supply	$2V_g$	=	$28V - 32V$
Load current	I_0	=	$0.2A - 0.9A$
Output voltage	V_0	=	$110V$
Converter resonant frequency	f_0	=	$50\,kHz$
Maximum output Power	P_0	=	$100W$

From a design stand-point, the condition with minimum DC supply voltage and maximum load current represents the worst case. Thus we will design the converter so as to give satisfactory performance in this case. The main steps in the converter tlesign are listed below.

1. In Fig. 2.7 locus of switching points are plotted for constant I_{n0}, constant ill and constant y in the $v_{nc} - i_{nl}$ plane. i.e., the values of v_{nc} and i_{nl} corresponding to the intersection of the three curves represent the points at which the power switches are turned off for those parametric values. From Fig. 2.7 pick **a** proper value of γ and 111 so that tlie converter operates in a region away from $\gamma = 180"$ or $f_{sn} = 1.0$. We will choose the following parameters corresponding to the point marked in tlie switching point diagram.

$$M = 0.9 \qquad f_{sn} = 1.08$$

2. With γ and M specified, Q can be obtained from Fig. 2.5 and I_{n0} from Fig. 2.7 as

$$Q = 2.25$$
$$I_{n0} = 2.0$$

3. The transformer turns ratio is obtained from the following equation.

$$n = \frac{V_{gmin}}{V_0 + 2V_D} M \approx \frac{1}{9}$$

where V_D is the voltage drop across one of the output rectifier diodes.

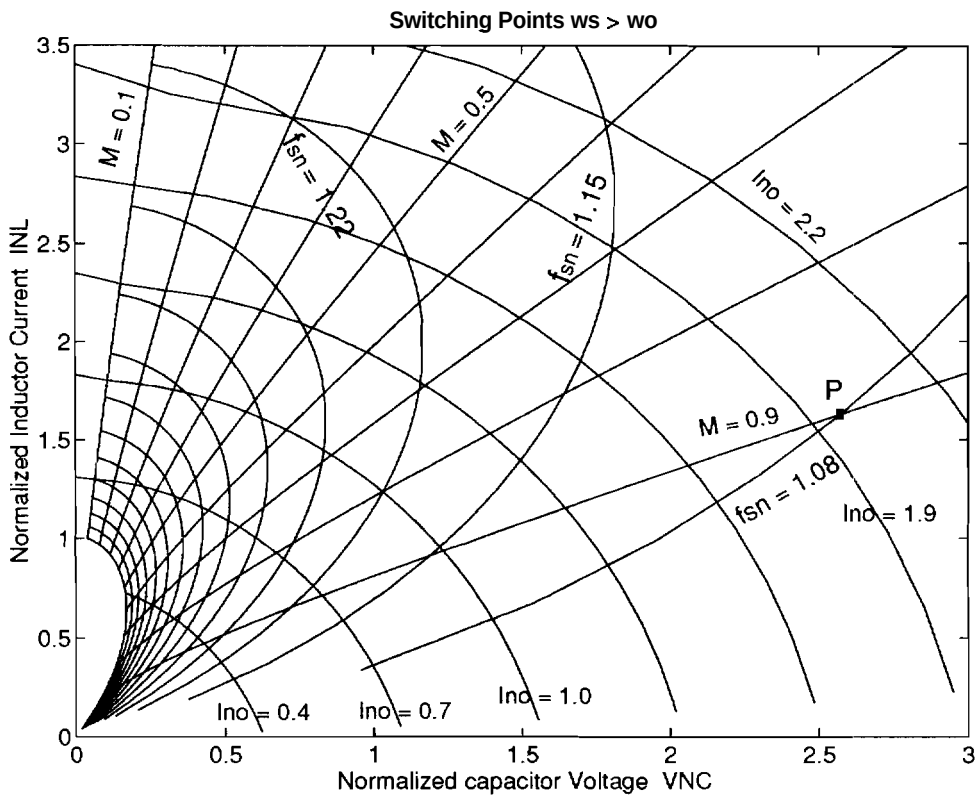

Figure 2.7 Locus of switching points for constant M, γ and I_{n0}

4. By definition, $I_{n0} = I_0 Z_0 / V_g$. Thus Z_0 can be obtained as

$$Z_0 = \frac{I_{n0} V_{gmin}}{I_0/n} \approx 3.5\,\Omega$$

Using a nominal value of f_0 of 50 kHz, the value of the resonant capacitor and inductor can be obtained as

$$C = \frac{1}{2\pi f_0 Z_0} = 0.91\mu F \approx 0.94\,\mu F$$
$$L = \frac{Z_0}{2\pi f_0} = 11.14\mu H \approx 10.3\,\mu H$$

With C = 0.94 μF and L = 10.3 pH, the actual resonant frequency becomes

$$f_0 = \frac{1}{2\pi\sqrt{LC}} = 51.15\,\text{kHz}$$

In order to determine the change in switching frequency because of line and load variations in the above design, we will consider the following four operating conditions.

Case I Minimum input voltage and maximum output current

This corresponds to the design case which is the worst condition expected. Here the switching frequency will be

$$f_s = \frac{\pi f_0}{\gamma} = 55.2\,kHz$$

Case II Minimum input voltage and minimum output current

Here we have

$$I_{0min} = 0.2A$$
$$I_{n0min} = \frac{I_0}{nV_g/Z_0} = 0.45$$

Since V_{n0} = 0.9, from the switching locus diagram in Fig. 2.7 we have the new value of f_{sn} as 1.32

$$\text{Hence } f_s = 1.32 f_0 = 67.5\,kHz$$

Case III Maximum input voltage and maximum output current

Here we have $V_g = 16V$. Hence

$$I_{n0max} = \frac{Z_0 I_{0max}}{n V_{gmax}} = 2.0$$
$$M_{min} = \frac{V_{gmin}}{V_{gmax}} M = 0.7875$$

where M_{min} is the converter gain in this case. Then from Fig. 2.7 $f_{sn} = 1.12$

$$f_s = 1.12 f_0 = 57.3\,kHz$$

Case IV Maximum input voltage and minimum output current

Here we have

$$V_g = 16V \Rightarrow M = 0.7875$$
$$I_{0min} = 0.2A \Rightarrow I_{n0min} = \frac{Z_0 I_{0min}}{n V_{gmax}} = 0.39$$

Thus $f_{sn} = 1.5 \Rightarrow f_s = 1.5 f_0 = 76.7\,kHz$ Thus in order to regulate the output against line and load variations, this design needs a variation in switching frequency of about 20 kHz.

The converter designed above was simulated under full load conditions. Fig. 2.3 and Fig. 2.4 are obtained from this simulation. Other variables of interest, especially the switch stresses and output variables are plotted in Appendix A. A step change in the load condition is also simulated with the load stepped to twice the full load, a level of loading that, is beyond the designed range. As seen from Fig. A.4, the state plane diagram for this case, the inductor current and capacitor voltage are quite high.

To verify the results in theory and simulation. a converter was fabricated based on the above design. The circuit which was laid out as well as the design of auxiliary components are given in Appendix A. MC34066, a variable frequency controller for resonant mode converters from Motorola is used as the feedback controller. A ground plane was used to reduce the effect of noise on the power supply. The measured

efficiency varied from 88% at full load to 80% at light loads. We had used an oversized core for the resonant inductor. Otherwise the efficiency could have been higher. The variations in the measured efficiency and switching frequency due to load variations are plotted in Appendix A for constant input voltage.

2.3 Operation Below Resonance

The operation of the converter below resonance is in many respects similar to its operation above resonance. In this case the switches turns off at zero voltage and zero current while they turn on to switch a finite current. But the diodes are force commutated. Again there are four different modes in the operation of the converter depending on the device conducting. As done before, a state plane diagram can be drawn from the equations representing these modes and is shown in Fig. 2.8. Here we need the initial switching points since the switches turn off naturally. Expressions similar to those in the cast of above resonance operation can be derived for $V_{nM1}, V_{nM2}, i_{nl}(t_0)$ and $v_{nc}(t_0)$.

In order to derive the control characteristics we need to express M in terms of γ and Q. Proceeding as before it can be shown that here also

$$M = \frac{2V_{ncmax}}{\gamma Q} \qquad [2.45]$$

where $V_{ncmax} = 1 - M + V_{nM1}$. Substituting for V_{nM1} we get a quadratic in M which can be solved to get the control characteristics shown in Fig. 2.9.

The component stresses can he derived as before and it is found that for similar operating conditions, the devices are subjected to a higher stress in the case of operation below resonance. The converter desigued in the above section was simulated to operate below resonance. Fig. 2.8 shows the state plane diagram in this case. As seen from the figure, the devices are subjected to a higher stress when operated below resonance.

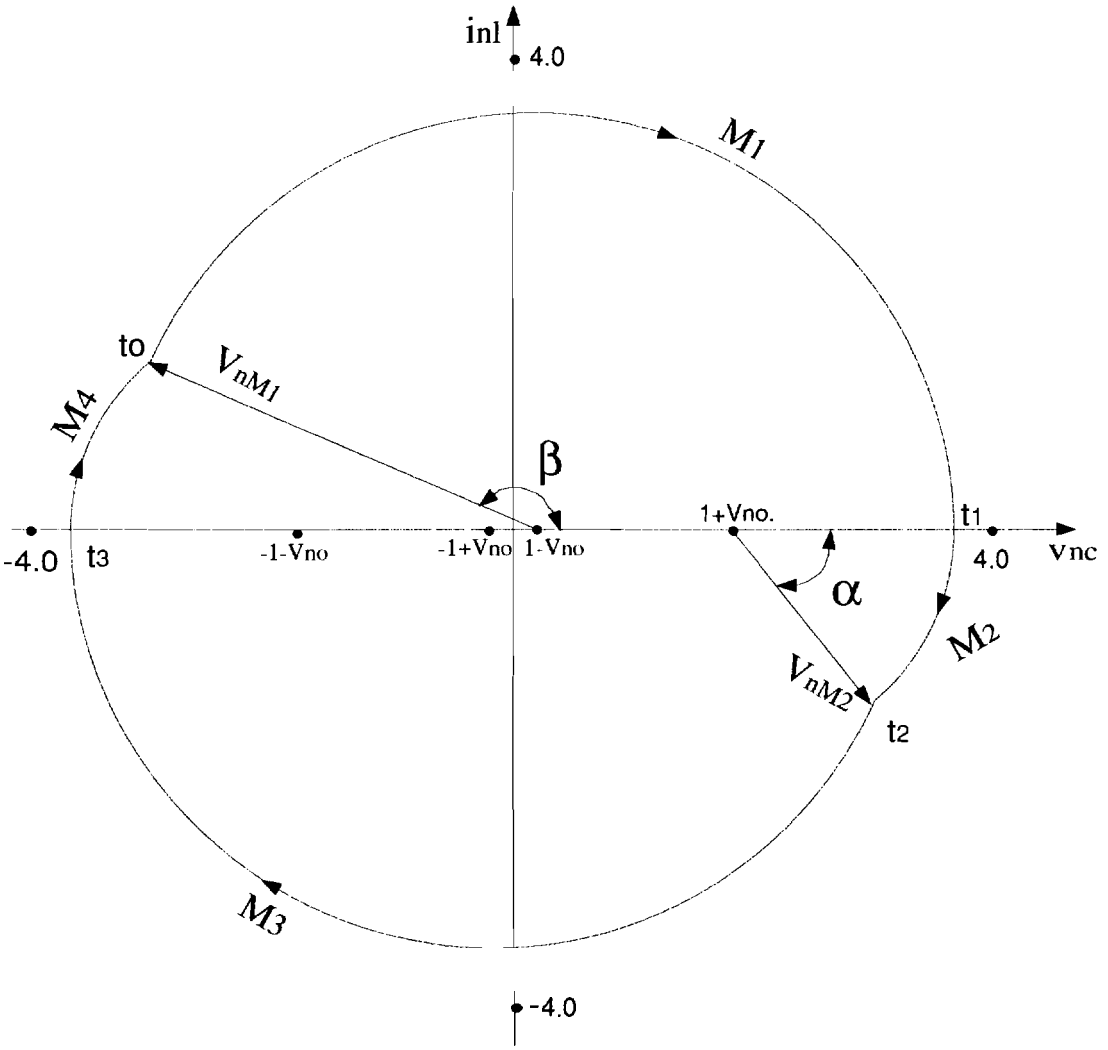

Figure 2.8 SRC state plane diagram for $f_s < f_0$

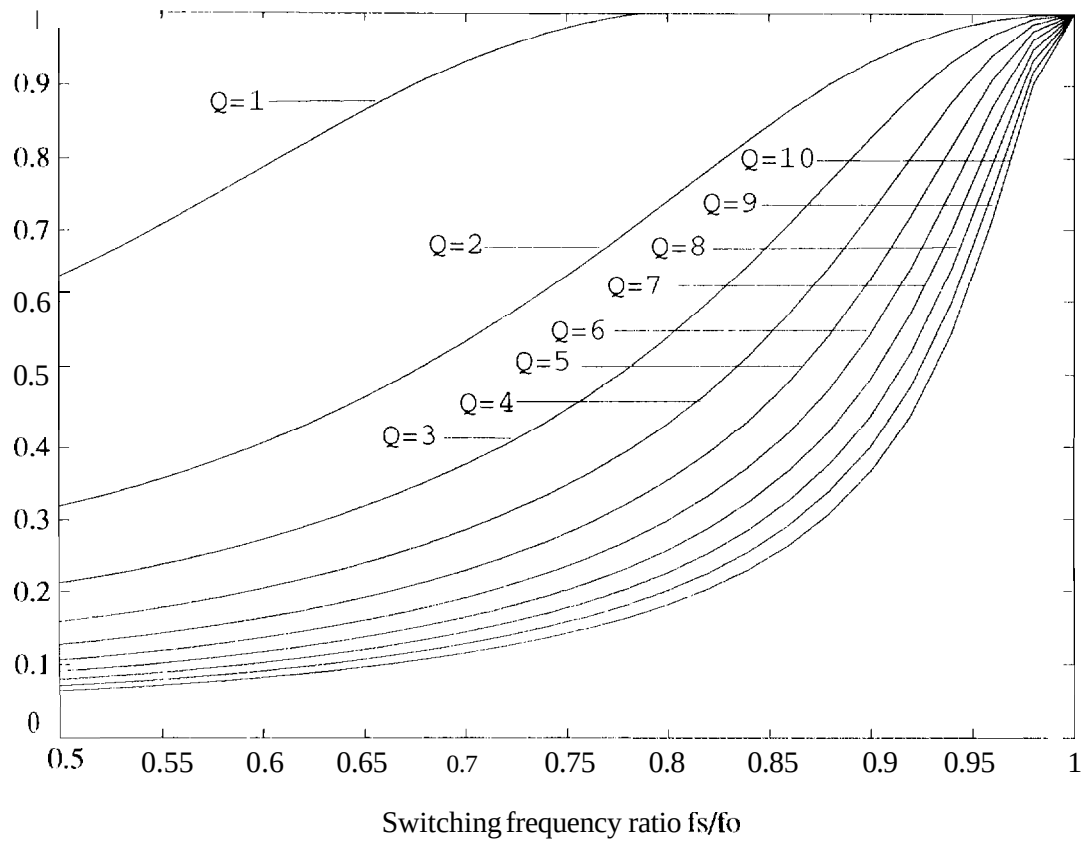

Figure 2.9 SRC control characteristic curves for $f_s < f_0$

2.3 Advantages of Operation Above Resonance

Here the operation of the series resonant converter above and below resonance is compared to bring out the relative merits.

As pointed out earlier when operated above resonance there are no turn on losses for tlie power switches while they have turn off losses. But note that the switches turn on not only at zero current but also at zero voltage. Hence it is possible to use lossless snubber capacitors across the switches. This can be clone because the capacitor discharges not at the turn-on of the switch but when the opposite switch turns off. When power MOSFETs operate at high frequencies, significant energy is stored in tlie drain-source and drain-gale capacitances and are internally discharged when the MOSFET turns on the next time. At higher voltages and frequencies this loss can be significant and constitutes a considerable portion of the switching losses. When the converter is operated above resonance. this loss is eliminated in the same way as before since the energy stored in the capacitances will be returned to the DC source as the opposite MOSFET turns off.

The diodes also turn off naturally when the current reverses due to the resonant action **of** the circuit and thus there is no loss associated with its turnoff. The diodes have a turn off time t_q equal lo the forward conduction time of the switch before forward voltage is applied. Hence these diodes need not have fast reverse recovery characteristics. This is a significant advantage since the parasitic diode of MOSFETs arc of only medium speed. Thus in this mode the parasitic diode of the power MOSFETs can be easily employed even at switching frequencies of hundreds of kHz. [Ste88]

Another important advantage of this mode of operation is that the output and input filter sizes are minimized since the frequency of operation is limited to a known lower limit.

All the above advantages are lost if the converter is operated below resonance. In this type of operation, there arc turn on losses for the power switches and tlie tliodes arc force commutated. Hence the tliodes must have very good reverse recovery

characteristics. Thus at high frequencies the parasitic diode associated with power MOSFETs cannot be used. Also the energy stored in the device capacitances is dissipated internally. Furthermore, in this mode of operation the switching frequency is lowered to control the output: the input and output, filters must be designed for tlie lowest frequencies encountered, as such thcv tend to he larger in size. The only advantage of operating below resonance is that the turnoff losses arc eliminated for the power switches. However, since turnoff losses can be reduced using the lossless snubber technique when operated above resonance, this seems to be the proper choice for high frequency power supply applications.

For switching frequencies less than $0.5f_0$, the converter operates in the discontinuous conduction mode. Also it is important to note that even in the frequency range $0.5f_0 \leq f_s \leq f_0$ which is the normal operating range for operation below resonance, there exists a discontinuous conduction mode. This can he seen from Fig. 2.9. When $Q = 1$, the gain becomes unity at a switching frequency of approximately $0.75f_0$ and is insensitive to variation in switching frequency thereafter. The reason is that the output bridge becomes reverse biased immediately after Q_1 conducts because the total voltage at the input side of the bridge is less than the output voltage. Consequently there is no diode conduction and the converter enters DCM[VC83]. This happens for low values of load Q. The boundary between DCM and CCM for this frequency range is given by

$$\begin{aligned} Q &< \frac{4}{\pi} f_{sn} \Rightarrow \text{DCM} \\ Q &> \frac{4}{\pi} f_{sn} \Rightarrow \text{CCM} \end{aligned}$$

So in the case of operation below resonance care must be taken so tliat the minimum load on the converter at any time is greater than the value given by the above expression. This is another disadvantage of operation below resonance since no such DC'M exists for frequency of operation above resonance.

2.5 Summary

The main advantages of SRC are

1. It has inherent short-circuit protection capability at all frequencies except the resonant frequency. Even at resonant frequency, since it takes a few resonant cycles for the current to rise to high values, there is considerable time for the control circuit to take corrective action.

2. The currents in the power devices as well as other circuit components decreases as the loacl decreases. Hence the conduction losses decreases as the load decreases yielding high part-load efficiency.

Its disadvantages are

1. The output voltage cannot be regulated for the no-load case. This can be seen from figures 2.5 and 2.9. As Q approaches 1, the curves have very little selectivity. At no-load the curve would simply be a horizontal line. This implies that the converter can be used only in applications where no-load regulation is not required.

2. Since the output at the rectificr is a current source drive, the DC' filter capacitor at the output must carry high ripple current(approximately half the DC output current). Because of this reason SRC' is considered more suitable for high-output-voltage, low-output-current rather than low-output-voltage, high-output-current.

3. The switching frequency varies directly with a change in loading and this results in poor cross-regulation in multi-output power supplies.

4. If both the load and the input voltage vary, the excursion of f_s can be large and it is clifficult to obtain goocl transient response.

5. It can operate only as a step-down converter. Hence to obtain a higher output voltage than the input, a transformer must be used.

3. PARALLEL RESONANT CONVERTER

3.1 Circuit Operation

A conventional half-bridge parallel resonant converter(PRC) with capacitive coupling is shown in Fig. 0.1. The diode transistor circuits $D_1 - Q_1$ and $D_2 - Q_2$ act like a pair of bidirectional switches operated at 50% duty ratio over one switching period T_s. Thus tlic resonant circuit in the converter is alternately excited by $+V_g$ and $-V_g$ in each half of a switching period. For continuous conduction mode operation, we can represent the effect of switching transistors by means of an equivalent square wave voltage source V_s with amplitude equal to $\pm V_g$. Furthermore, because of tlic fact that the AC to DC power conversion is achieved by rectifying the voltage across the resonant capacitor, a large filtering inductance L_0 is needed to minimize the loading effect of the output circuit. As seen from Fig. 3.1, the current input to the bridge rectifier has constant amplitude $+I_0$ and $-I_0$, depending on whether the resonant capacitor voltage $v_c(t)$ is positive or negative. Thus the effect of the DC output on the input circuit can be represented by a constant current source $i_E(t)$ with its polarity depending on the sign of the coupling capacitor voltage.

3.2 Operation Above Resonance

The assumptions of section 2.2 are valid here also. As with the case of series resonant converter, in this mode of operation the switches arc force commutated. But they turn on at zero voltage and zero current. The diodes arc again naturally commutated. Turn-off losses exist for tlic power switches. The operation of the converter over one switching period can be divided into four intervals wherein the circuit modes are distinct. These circuit modes and their corresponding equations

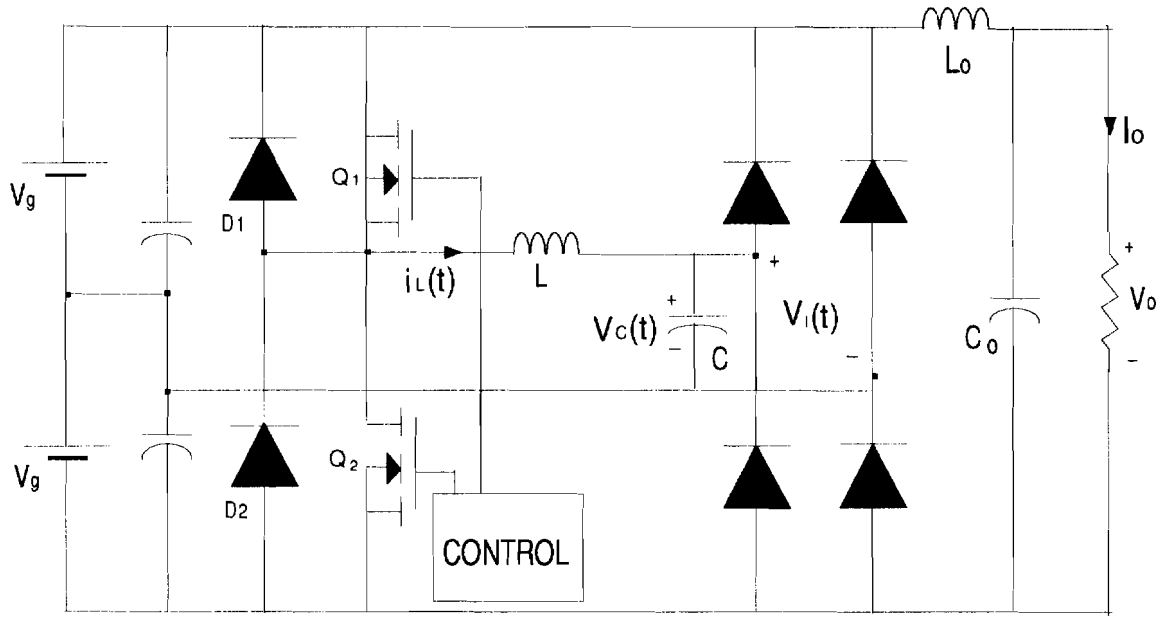

Figure 3.1 Conventional PRC' circuit diagram

are derived below.

Mode 1 $t'' \leq t \leq t_2$

At t_0, Q_2 is turned off at a finite current. The negative inductor current is maintained by diode D_1 while Q_1, Q_2 and D_2 are off. The circuit can be reduced as the one shown in Fig. 3.2(a). At t_1, D_1 turns off naturally as the inductor current goes through zero. Q_1 turns on and carries the positive inductor current and the circuit of Fig. 3.2(a) is still valid. The governing equations for this mode normalized as before are

$$\frac{di_{nl}(t)}{dt} = \omega_0 \left(1 - v_{nc}(t)\right) \quad [3.1]$$

$$\frac{dv_{nc}(t)}{dt} = \omega_0 \left(i_{nl}(t) + I_{n0}\right) \quad [3.2]$$

where ω_0 is the resonant frequency in rad/sec. By combining 3.1 and 3.2 we get

$$\frac{di_{nl}}{dv_{nc}} = \frac{1 - v_{nc}}{i_{nl} + I_{n0}} \quad [3.3]$$

Mode 2 $t_2 \leq t \leq t_3$

At t_2, the resonant capacitor voltage becomes zero going positive. The output current also reverses direction. The equivalent circuit for this case is shown in Fig. 3.2(b). The state plane equation for this mode is

$$\frac{di_{nl}}{dv_{nc}} = \frac{1 - v_{nc}}{i_{nl} - I_{n0}} \quad [3.4]$$

Mode 3 $t_3 \leq t \leq t_5$

At t_3, Q_1 is forced to turn off. D_2 turns on to maintain the continuity of current in the inductor. At t_4, D_2 turns off naturally and Q_2 starts conduction. The corresponding equivalent circuit is shown in Fig. 3.2(c). This mode is described by

$$\frac{di_{nl}}{dv_{nc}} = \frac{-1 - v_{nc}}{i_{nl} - I_{n0}} \quad [3.5]$$

Mode 4 $t_5 \leq t \leq t_0 + T_s$

At, t_5, the resonant capacitor voltage again becomes zero reversing the direction of

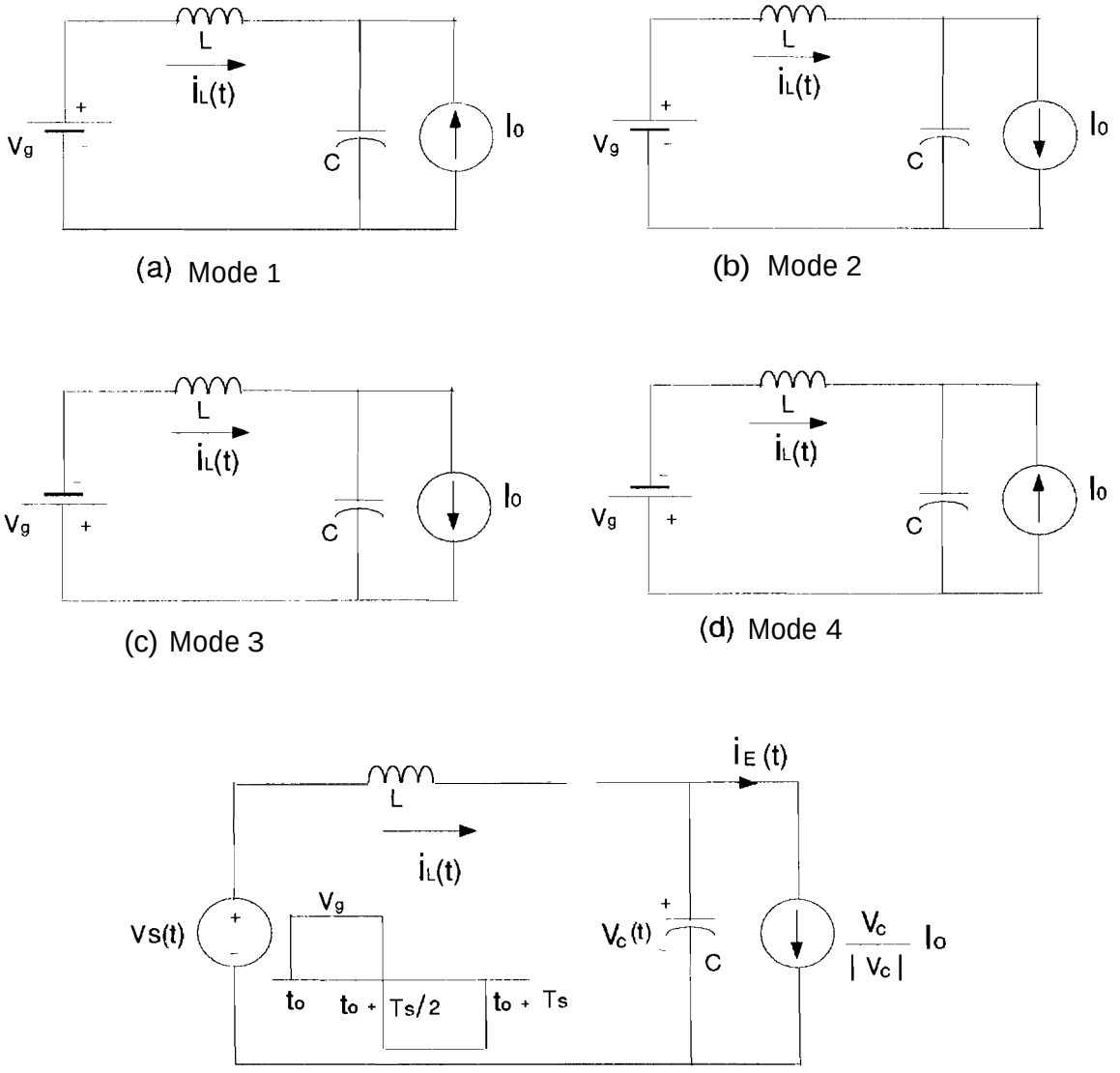

(e) PRC equivalent circuit

Figure 3.2 Four modes in the operation of PRC

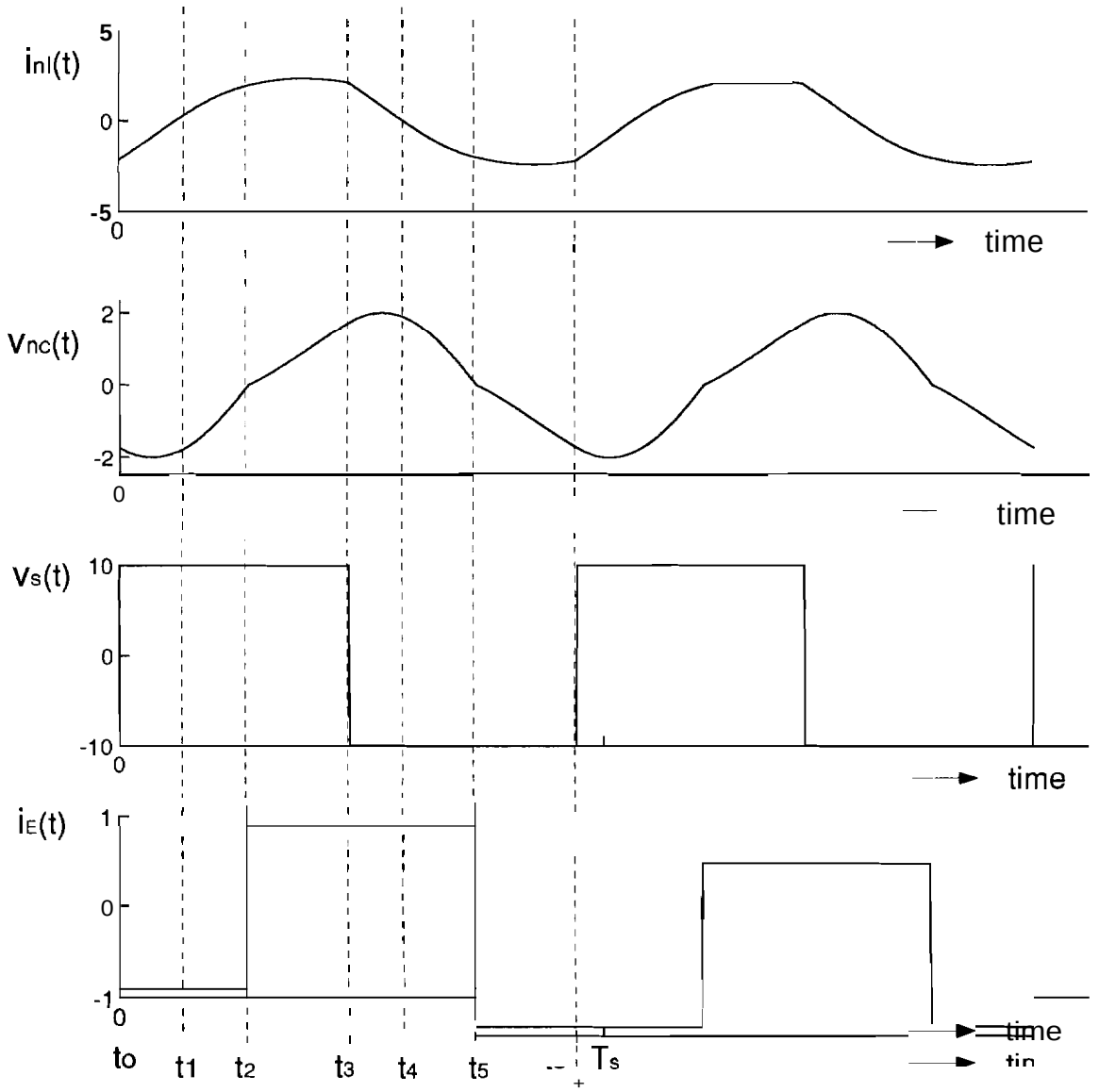

Figure 3.3 Steady state waveforms in continuous conduction mode

the output current. The circuit reduces to the one shown in Fig. 3.2(d). The corresponding state plane equation is

$$\frac{di_{nl}}{dv_{nc}} = \frac{-1 - v_{nc}}{i_{nl} + I_{n0}} \qquad [3.6]$$

This cycle is repeated after $t_0 + T_s$ when Q_2 is force commutated and D_1 turns on. From the above analysis the equivalent circuit shown in Fig. 3.2(e) is obtained. Typical steady state voltage and current waveforms are shown in Fig. **3.3.**

3.2.1 State Plane Analysis

The steady state response of the half-bridge PRC with capacitive coupling can be determined from the equivalent circuit, shown in Fig. 3.2(e). The driving source $V_g s(t)$ is given by the product $V_g s(t)$ where s(t) is a square wave with period T_s and amplitude of ± 1, which represent the switching action of $Q_1 - D_1$ and $Q_2 - D_2$. In the PRC, AC to DC power conversion is accomplished with the resonant capacitor voltage $v_c(t)$. The output voltage V_0 is equal to the average value of the rectified $v_c(t)$. As seen from Fig. 3.2(e), $i_E(t)$ is a dependent current source with current polarity determined by the sign of $v_c(t)$ such that the average power dissipated in it is equal to the DC output power of the converter.. We can represent $i_E(t)$ as

$$i_E(t) = \frac{v_c(t)}{|v_c(t)|} I_0 \qquad [3.7]$$

where $|v_c(t)|$ is the magnitude of $v_c(t)$ and I_0 is the *DC* output current. The output voltage V_0 can be determined by

$$V_0 = \frac{1}{T_s} \int_0^{T_s} |v_c(t)| dt \qquad [3.8]$$

The state plane equations for the four modes derived in the above section can be obtained directly from Fig. 3.2(e). The state plane equation for this circuit with normalized quantities is

$$\frac{di_{nl}(t)}{dv_{nc}(t)} = \frac{v_{ns}(t) - v_{nc}(t)}{i_{nl}(t) - i_{nE}(t)} \qquad [3.9]$$

where $v_{nc}(t)$ and $i_{nl}(t)$ are defined as before and

$$v_{ns}(t) = \frac{v_s(t)}{V_g} \qquad i_{nE}(t) = \frac{Z_0 i_E(t)}{V_g}$$

where Z_0 is again the characteristic impedance of the resonant circuit.

Equation 3.9 is nonlinear but can be solved by a piecewise linear analysis over intervals of the switching period T_s. It can be shown that the solution consist of four circular arcs in the $i_{nl} - v_{nc}$ state plane and are given by

$$[v_{nc}(t) - v_{nsi}]^2 + [i_{nl}(t) - i_{nEi}]^2 = V_{nMi}^2 \qquad [3.10]$$

where i = 1,2,3,4. The centers of these circular arcs correspond to the singular point of equation 3.9 and are determined by the value of s(t) and the sign of $i_{nE}(t)$ over a switching period T_s. As seen from Fig. 3.2 and Fig. 3.3, each singular point correspond to one of the time intervals listed below.

$$\begin{aligned}
(v_{ns1}, i_{nE1}) &= (+1, -I_{n0}) \qquad t_0 \le t < t_2 \\
(v_{ns2}, i_{nE2}) &= (+1, +I_{n0}) \qquad t_2 \le t < t_3 \\
(v_{ns3}, i_{nE3}) &= (-1, +I_{n0}) \qquad t_3 \le t < t_5 \\
(v_{ns4}, i_{nE4}) &= (-1, -I_{n0}) \qquad t_5 \le t < t_0 + T_s
\end{aligned}$$

Thus V_{nMi} and can be expressed as

$$V_{nM1}^2 = V_{nM3}^2 = [v_{nc}(t_0) - 1]^2 + [i_{nl}(t_0) + I_{n0}]^2 \qquad [3.11]$$

$$V_{nM2}^2 = V_{nM4}^2 = [v_{nc}(t_2) + 1]^2 + [i_{nl}(t_2) - I_{n0}]^2 \qquad [3.12]$$

Refering to 3.9, we can construct the state plane diagram which is shown in Fig. 3.4 for the converter operating in CCM. The DC output voltage V_0 is obtained by taking the average value of the resonant capacitor voltage. Since $v_c(t)$ and $i_l(t)$ are symmetrical with respect to half the switching period, V_0 can be evaluated as

$$V_0 = \frac{2}{T_s} \int_{t_0}^{T_s/2} |v_c(t)| dt \qquad [3.13]$$

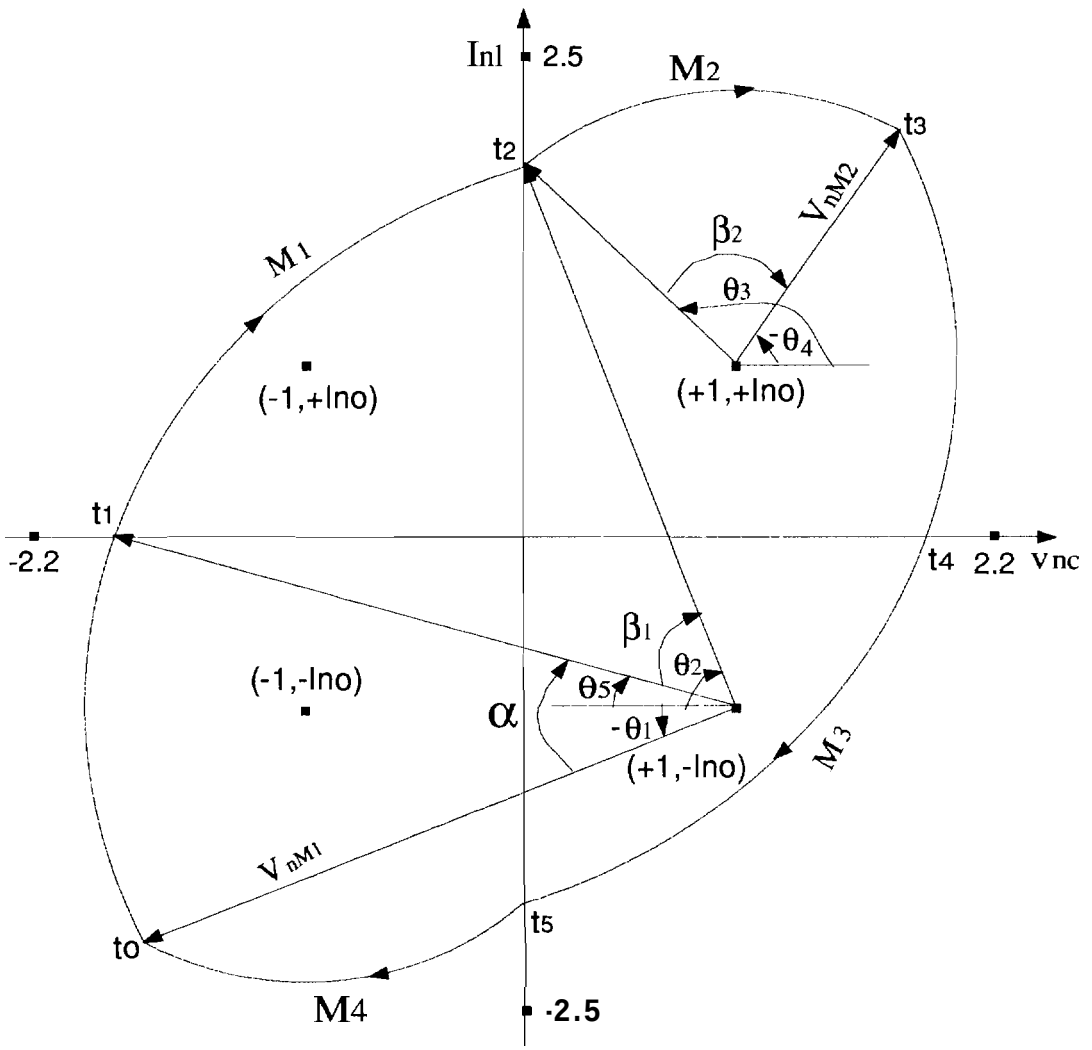

Figure 3.4 PRC state plane diagram for $f_s > f_0$

Based on the circuit diagram in Fig. 3.1 and the state plane diagram in Fig. 3.4,

$$v_c(t) = \begin{cases} -V_g + L\frac{di_l}{dt} & t_0 \le t \le t_2 \\ V_g - L\frac{di_l}{dt} & t_2 \le t \le t_0 + T_s/2 \end{cases} \quad [3.14]$$

Substituting equation **3.14** into **3.13,** we can obtain the average output voltage which is given by

$$V_0 = \frac{1}{\gamma}[2Z_0 i_l(t_2) - V_g(\gamma - 2\beta_2)] \quad [3.15]$$

where

$$\beta_2 = \omega_0(t_3 - t_2) \quad [3.16]$$

$$\omega_0 = \frac{1}{\sqrt{LC}} \quad [3.17]$$

$$\gamma = \alpha + \beta_1 + \beta_2 = \pi f_0/f_s \quad [3.18]$$

In terms of normalized quantities, **3.15** can be written as

$$V_{n0} = \frac{1}{\gamma}[2i_{nl}(t_2) - (\gamma - 2\beta_2)] \quad [3.19]$$

where $i_{nl}(t_2)$ is the normalized value of $i_l(t_2)$. The average input current from the source is given by

$$I_g = \frac{2}{T_s}\int_{t_0}^{t_0+T_s/2}\left(C\frac{dv_c}{dt} + i_E\right)dt \quad [3.20]$$

After some steps of manipulation, equation **3.20** becomes

$$I_g = \frac{1}{\gamma}[-2\omega_0 C v_c(t_0) - I_0(\gamma - 2\beta_2)] \quad [3.21]$$

which upon normalization becomes

$$I_{ng} = \frac{1}{\gamma}[-2v_{nc}(t_0) - I_{n0}(\gamma - 2\beta_2)] \quad [3.22]$$

Since we assume that the resonant circuit is lossless, the average power input to the converter must be equal to the DC power output to the load. Equating $V_0 I_0$ to $V_g I_g$ and $V_{n0} I_{n0}$ to $V_{ng} I_{ng}$ we obtain the following relations.

$$\frac{v_{nc0}}{i_{nl2}} = -I_{n0} \quad [3.23]$$

$$\frac{V_0}{V_g} = -R_0\frac{C}{L}\frac{v_{c0}}{i_{l2}} \quad [3.24]$$

where R_0 is the load resistance and i_{l2} and v_{c0} are the resonant inductor current at time t_2 and the resonant capacitor voltage at time t_0 respectively. The suffix n on currents ancl voltages represent normalized quantities. Substituting **3.23** into **3.24** we get

$$V_{no} = \frac{R_0}{Z_0} I_{n0} = Q_p I_{n0} \qquad [3.25]$$

where $Q_p = R_0/Z_0$ is the loaded quality factor of the parallel resonant circuit. Normalized output voltage can be obtained in terms of γ, β_2 ancl v_{nc0} by combining **3.19** and **3.23** as

$$V_{n0} = \frac{1}{\gamma}[-(\gamma - 2\beta_2) - \frac{2v_{nc0}}{I_{n0}}] \qquad [3.26]$$

3.2.2 Control Characteristics

The control characteristics are very useful in converter design. For a given normalized output current I_{n0}, the relation between v_{nc0} and i_{nl0} can he derived from 3.10. Equating V_{nM1} from **3.10** with t = t_0 and t = t_2 and using **3.23,** we obtain

$$v_{nc0} = -\sqrt{\frac{I_{n0}^4 - I_{n0}^2(i_{nl0} + I_{n0})^2}{I_{n0}^2 - 1}} \qquad [3.27]$$

From the state plane diagram shown in Fig. 3.4 it can be seen that

$$\alpha + \beta_1 = \theta_2 - \theta_1 \qquad [3.28]$$

Thus

$$\tan(\alpha + \beta_1) = \tan(\theta_2 - \theta_1) = \frac{\tan\theta_2 - \tan\theta_1}{1 + \tan\theta_2 \tan\theta_1} \qquad [3.29]$$

where

$$\tan\theta_1 = \frac{i_{nl0} + I_{n0}}{1 - v_{nc0}} \qquad [3.30]$$

$$\tan\theta_2 = i_{nl2} + I_{n0} \qquad [3.31]$$

From 3.30 and 3.31 we obtain

$$\tan(\alpha + \beta_1) = \frac{(1 - v_{nc0})(i_{nl2} + I_{n0}) - (i_{nl0} + I_{n0})}{(1 - v_{nc0}) + (i_{nl2} + I_{n0})(i_{nl0} + I_{n0})} \qquad [3.32]$$

Similarly, the following relations can also be obtained from Fig. **3.4.**

$$\tan\theta_3 = I_{n0} - i_{nl2} \qquad [3.33]$$

$$\tan\theta_4 = \frac{I_{n0} + i_{nl0}}{-(1 + v_{nc0})} \qquad [3.34]$$

$$\tan\beta_2 = \tan(\theta_3 + \theta_4) = \frac{(I_{n0} - i_{nl2})(v_{nc0} + 1) - (I_{n0} + i_{nl0})}{(1 + v_{nc0}) + (I_{n0} - i_{nl2})(I_{n0} + i_{nl0})} \qquad [3.35]$$

From 3.18 we can write

$$\tan\gamma = \tan[(\alpha + \beta_1) + \beta_2] \qquad [3.36]$$

$$= \frac{\tan(\alpha + \beta_1) + \tan\beta_2}{1 - \tan(\alpha + \beta_1)\tan\beta_2} \qquad [3.37]$$

Substituting **3.32** and **3.3.5** into **3.37** and eliminating i_{nl2} and v_{nc0} using **3.23** and **3.27** we can express $\tan\gamma$ in terms of I_{n0} and i_{nl0}.

For a given normalized output current I_{n0} and switching frequency ratio y, the normalized initial inductor current i_{nl0} can he determined using **3.37.** v_{nc0} and i_{nl2} can be found from 3.27 and 3.23, respectively. The state plane parameter β_2 is related to I_{n0}, i_{nl0}, i_{nl2} and v_{nc0} by equation 3.35. Then the voltage gain M which is the normalized output voltage V_{n0} can he determined using 3.26. The relationship curves between voltage gain M, switching frequency ratio γ and normalized output current I_{n0} are plotted in Fig. **3.5.** Since $M = Q_p I_{n0}$, Q_p also can be found out. Thus, if any two variables among M, y, Q_p and I_{n0} are known, the remaining two can be determined. Since it is very difficult to obtain a closed form expression for M in terms of y and Q_p from equation **3.37** an approximate formula which is quite accurate for operation above resonance is used to obtain the control characteristics between these variables [Ste88]. This is plotted in Fig. **3.6.** Actually. any one of these two figures is sufficient for the purpose of designing the converter.

3.2.3 Component Stresses

As with the case of the series resonant converter, we can derive the component stresses analytically based on the state plane diagram and the operating conditions

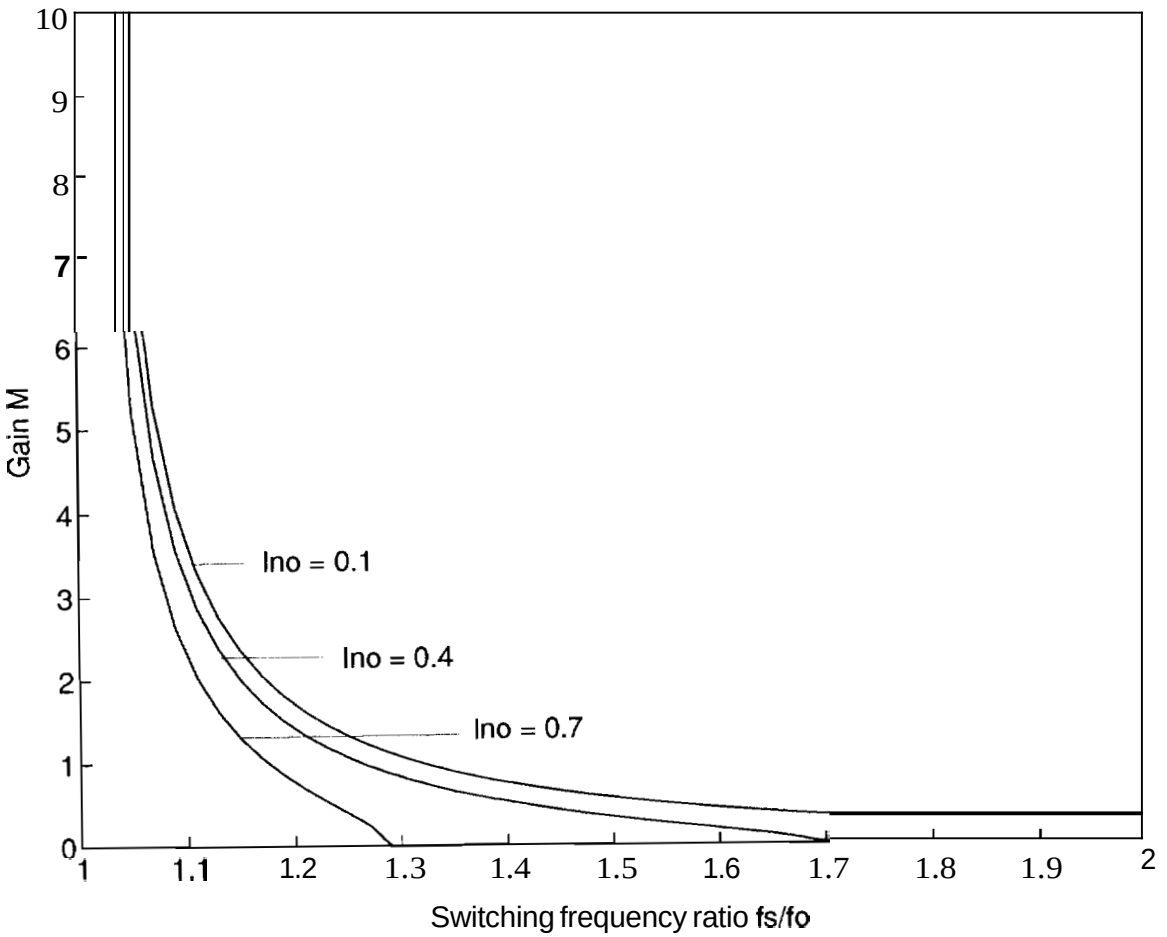

Figure 3.5 PRC control characteristic curves: (M, f_{sn}, I_{n0})

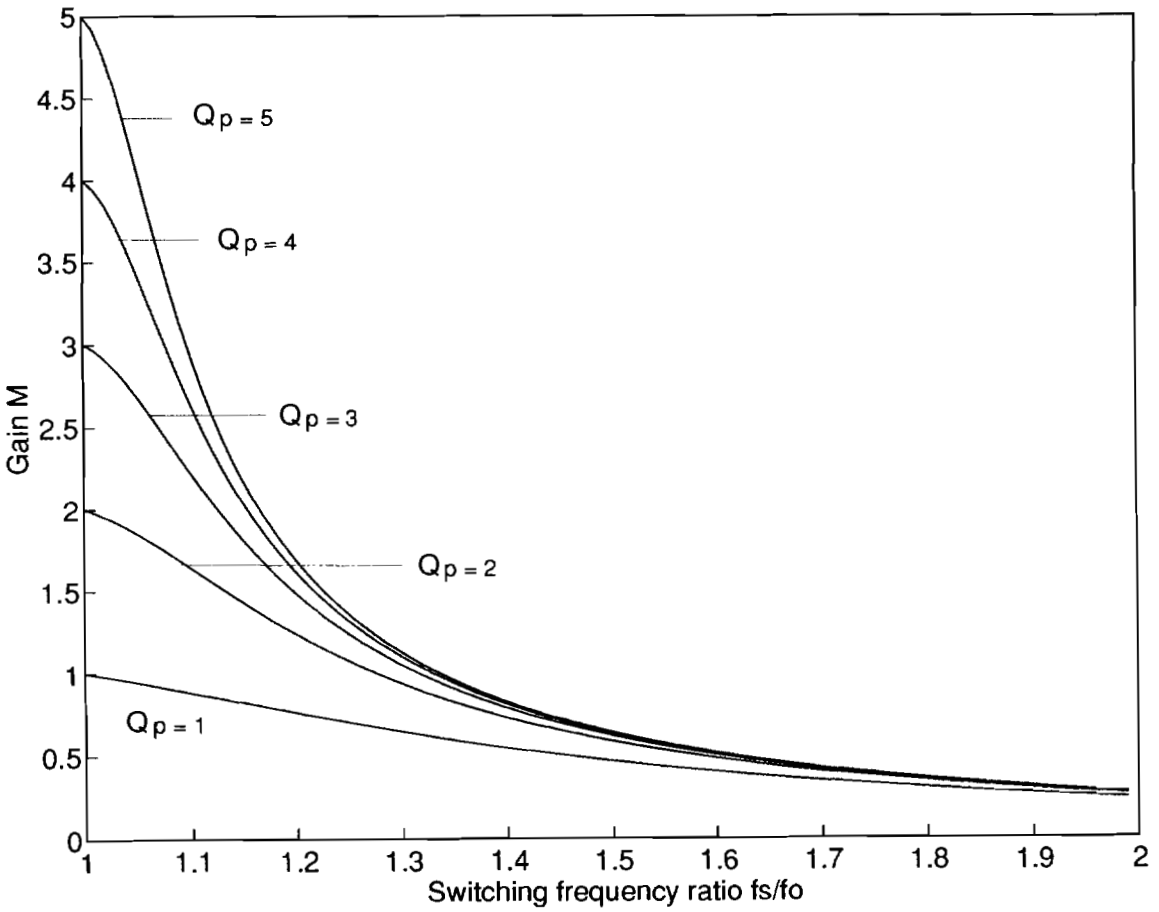

Figure 3.6 PRC control characteristic curves: (M, f_{sn}, Q_p)

of the converter. The average switch current can he calculated as

$$I_Q = \frac{2}{T_s}\int_{t_1}^{t_0+T_s/2} i_l(t)dt \qquad [3.38]$$

which when evaluated and normalized becomes

$$I_{nQ} = \frac{1}{\gamma}[I_{n0}(\beta_2 - \beta_1) - (v_{nc1} + v_{nc0})] \qquad [3.39]$$

To evaluate this we need β_1 and v_{nc1} which is the resonant capacitor voltage at time t_1. But from Fig. 3.4 v_{nc1} can he expressed as

$$v_{nc1} = -\left(\sqrt{V_{nM1}^2 - I_{n0}^2} - 1\right) \qquad [3.40]$$

β_1 can be found as

$$\beta_1 = \theta_2 - \theta_1 - \alpha \qquad [3.41]$$

where a can be found frotn

$$\alpha = \theta_5 - \theta_1 \qquad [3.42]$$

Hence

$$\tan\alpha = \frac{\tan\theta_5 - \tan\theta_1}{1 + \tan\theta_5 \tan\theta_1} \qquad [3.43]$$

and we have

$$\tan\theta_5 = \frac{I_{n0}}{1 - v_{nc1}} \qquad [3.44]$$

Similarly, the average current in each diode is given by

$$I_D = \frac{2}{T_s}\int_{t_0}^{t_1} -i_l(t)dt \qquad [3.45]$$

which upon evaluation and normalization becomes

$$I_{nD} = \frac{1}{\gamma}[I_{n0}\alpha - (v_{nc1} - v_{nc0})] \qquad [3.46]$$

From the state plane diagram the peak resonant capacitor voltage can be calculated

$$V_{ncmax} = \begin{cases} V_{nM1} - 1.0 & \text{if } |i_{nl0}| > I_{n0} \\ V_{nM2} + 1.0 & \text{otherwise} \end{cases} \qquad [3.47]$$

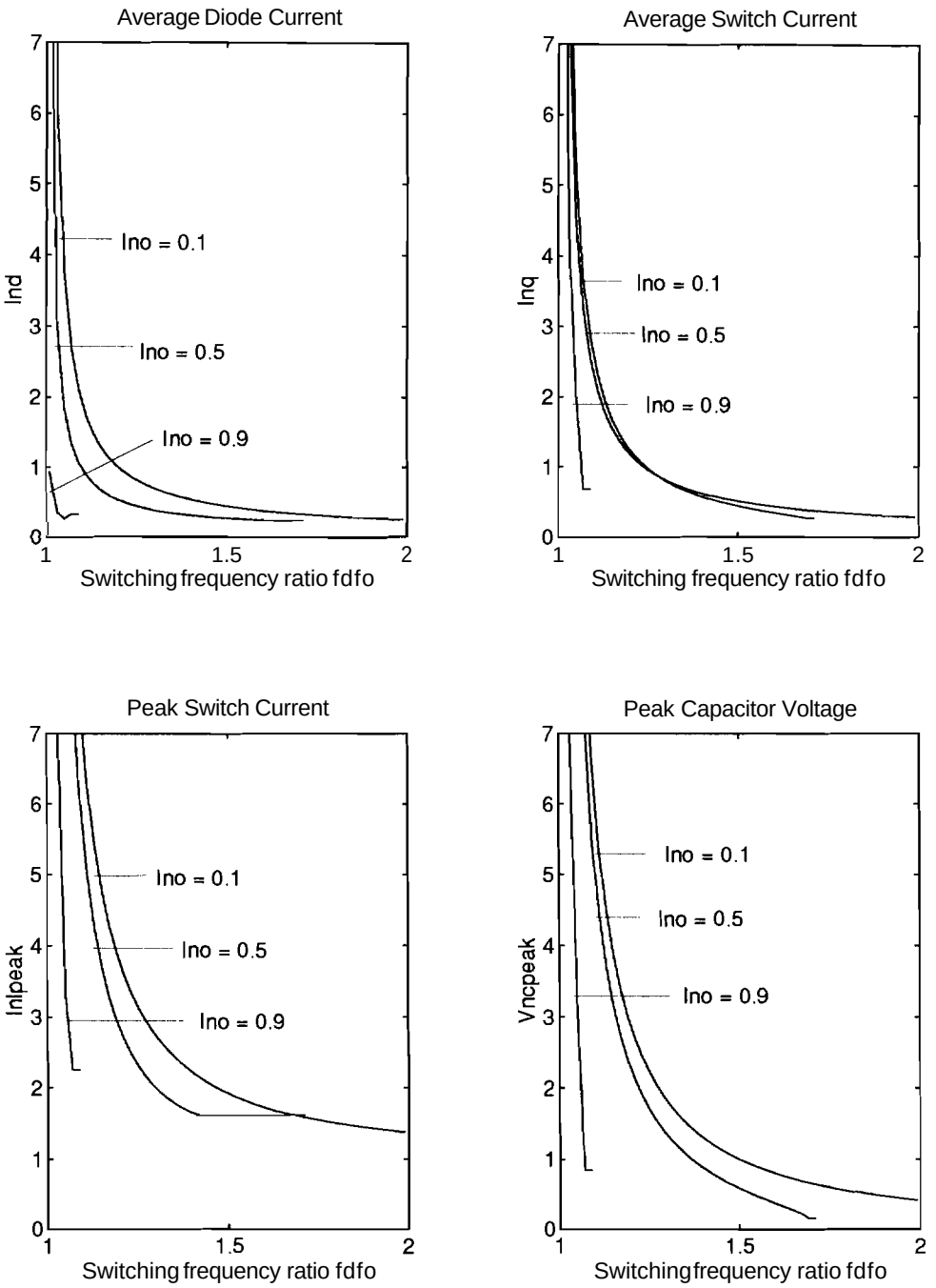

Figure 3.7 Component stresses as a function of switching frequency

To find the peak inductor current again note from Fig. 3.3 that

$$i_{nlmax} = \begin{cases} I_{n0} + V_{nM2} & \text{if } v_{nc0} \geq 1.0 \\ i_{nl0} & \text{otherwise} \end{cases} \qquad [3.48]$$

Thus i_{nlmax} can be obtainecl from the above equation. These quantities are plotted in Fig. 3.7 as a function of the switching frequency for different values of normalized output current I_{n0}. These quantities are plotted in Fig. 3.7 as a function of the switching frcquencv for different values of normalized output current I_{n0}.

3.2.4 Design of Converter

Here a simple method for designing a parallel resonant converter is illustrated. A complete design can be obtained by specifying any two among the four parameters M, Q, I_{n0} and y. Normally it is recommended that γ and M are specified so that the region of operation in the control characteristics under any loading conditions can be determined. We will design a converter with the following specifications.

Input DC supply	$2V_g$	=	$20V - 32\text{V}$
Load current	I_0	=	$25A - 2.0A$
Output voltage	V_0	=	$5V$
Converter resonant frequency	f_0	=	100 kHz
Maximum output power	P_0	=	$125W$

The design proceeds exactly as in the case of the series resonant converter. The worst case during the operation of the converter will occur when the input voltage is a minimum and the load current is maximum. We will take this as the design point. The main steps in the design are listed below.

1. 1n Fig. 3.8 locus of initial switching points are plotted for constant I_{n0}, constant, M and constant y in the $v_{nc} - i_{nl}$ plane. i.e., the values of v_{nc} and i_{nl} corresponding to the intersection of the three curves represent the points at which the power switches are turned off for those parametric values. From Fig. 3.8 pick a

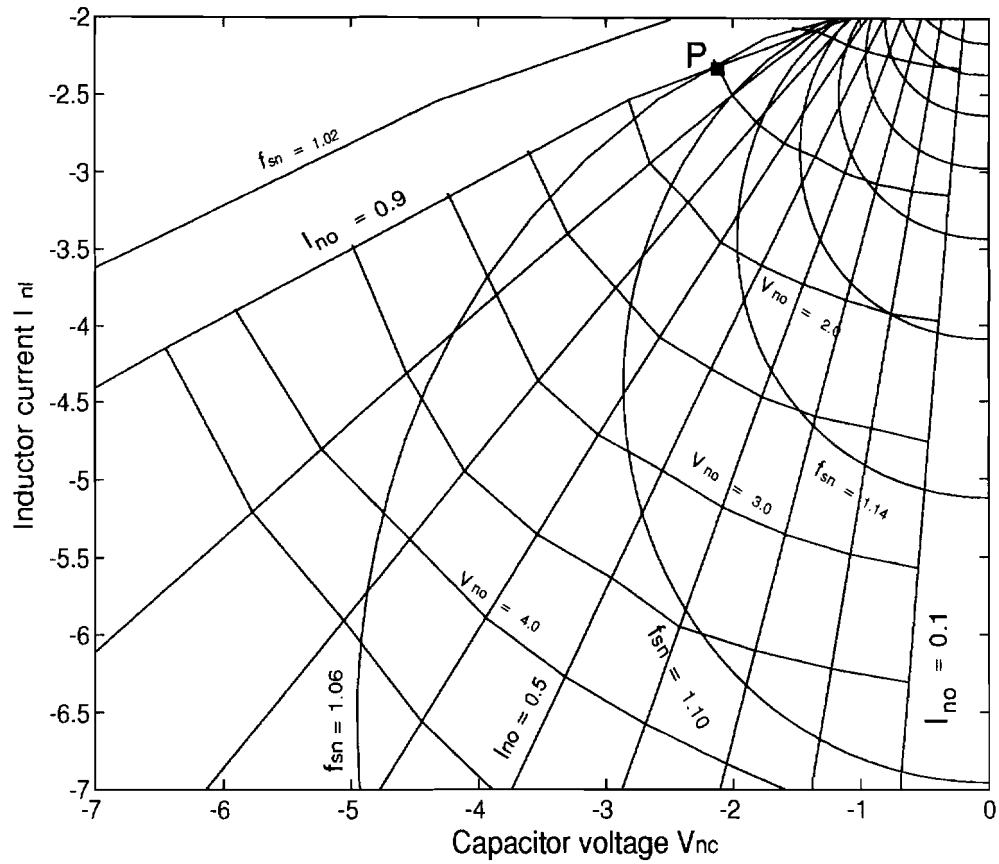

Figure 3.8 Locus of switching points for constant M, γ and I_{n0}

proper value of γ and M so that the converter operates in a region away from $\gamma = 180"$ or $f_{sn} = 1.0$. We will choose the following parameters corresponding to the point marked in the switching point diagram.

$$M = 0.9 \qquad f_{sn} = 1.08$$

With γ and M specified, I_{n0} can be obtained from Fig. 3.8 and Q_p from Fig. 3.6.

$$Q_p = 1.67$$
$$I_{n0} = 0.9$$

2. The transformer turns ratio is obtained from the equation given below.

$$n = \frac{V_{gmin}}{V_0 + 2V_D} M \approx 2.5$$

In the above equation V_D is the voltage drop across each of the output rectifier diodes and is assumed to be 0.5V.

3. Now Z_0 can be obtained as

$$Z_0 = \frac{I_{n0} V_{gmin}}{I_0/n} \approx 0.9\,\Omega$$

With $f_0 = 100\,\text{khz}$, the value of the resonant capacitor and inductor are

$$C = \frac{1}{2\pi f_0 Z_0} \approx 1.77\,\mu F$$
$$L = \frac{Z_0}{2\pi f_0} \approx 1.43\,\mu H$$

Since the required inductance is very low, the leakage inductance associated with the primary winding of the transformer can be effectively used as the resonant inductor.

Again, in order to find the change in switching frequency because of line and load variations in the above design, we can consider the following four operating conditions.

Case I Minimum input voltage and maximum output, current

This corresponds to the design case which is the worst condition expected. Here the switching frequency will be

$$f_s = f_{sn} f_0 = 106\,kHz$$

Case II Minimum input voltage and minimum output current

Here we have

$$I_{0min} = 2.0A$$
$$I_{n0min} = \frac{I_0}{nV_g/Z_0} = 0.07$$

Since $V_{n0} = 1.5$, from the switching locus diagram in Fig. 3.8 the new value of f_{sn} is 1.25. Hence

$$f_s = 1.25 f_0 = 125\,kHz$$

Case III Maximum input voltage and maximum output current

Here we have $V_g = 32V$. Hence

$$I_{n0max} = \frac{Z_0 I_{0max}}{nV_{gmax}} = 0.28$$
$$M_{min} = \frac{V_{gmin}}{V_{gmax}} M = 0.94$$

where M_{min} is the converter gain in this case. Then from Fig. 3.8 $f_{sn} = 1.32$.

$$f_s = 1.32 f_0 = 132\,kHz$$

Case IV Maximum input voltage and minimum output current

Here we have

$$V_g = 32V \Rightarrow M = 0.94$$
$$I_{0min} = 2A \Rightarrow I_{n0min} = \frac{Z_0 I_{0min}}{nV_{gmax}} = 0.02$$

Thus $f_{sn} = 1.35 \Rightarrow f_s = 1.35 f_0 = 135 kHz$.

This design although allows a variation of about **30** kHz in the switching frequency because of line and load variations, keeps the peak stresses to a minimum. If we allow a higher tolerance in the peak stresses on the devices, switching frequency variation can be reduced. The converter designed above was simulated under full load conditions. Fig. **3.3** and Fig. **3.4** are obtained from this simulation. Other variables of interest, especially the switch stresses and output variables are plotted in Appendix A. In order to verify tlie results from the analysis and simulation, a converter was breadboarded. The circuit waveforms were in close agreement with the results obtained from simulation. At full load the measured efficiency was 87%. Hut as the load on the converter decreased the efficiency also dropped. At **50%** load the efficiency was only around **70%.** The measured efficiency and switching frequency as a result of variations in load are plotted in Appendix A.

3.3 Operation Below Resonance

Operation of the converter below resonance can also be analyzed in a similar manner. In this case the switches turn off naturally but they have turn-on losses. The diodes are force commutated. The operation of the converter can be split up into four different modes. A state plane diagram can he drawn from the equations representing these modes and is shown in Fig. **3.9.**

The control characteristics can be derived after expressing γ in terms of i_{nl0} and I_{n0}. The gain M in this case is given by

$$M = \frac{1}{\gamma}[\gamma - 2\beta_1 - \frac{2v_{nc0}}{I_{n0}}] \qquad [3.49]$$

The control characteristics for operation below resonance is plotted in Fig. **3.10.**

The component stresses can be derived by making use of state plane parameters as before. It is found that the devices arc subjected to a higher stress in the case of operation below resonance.

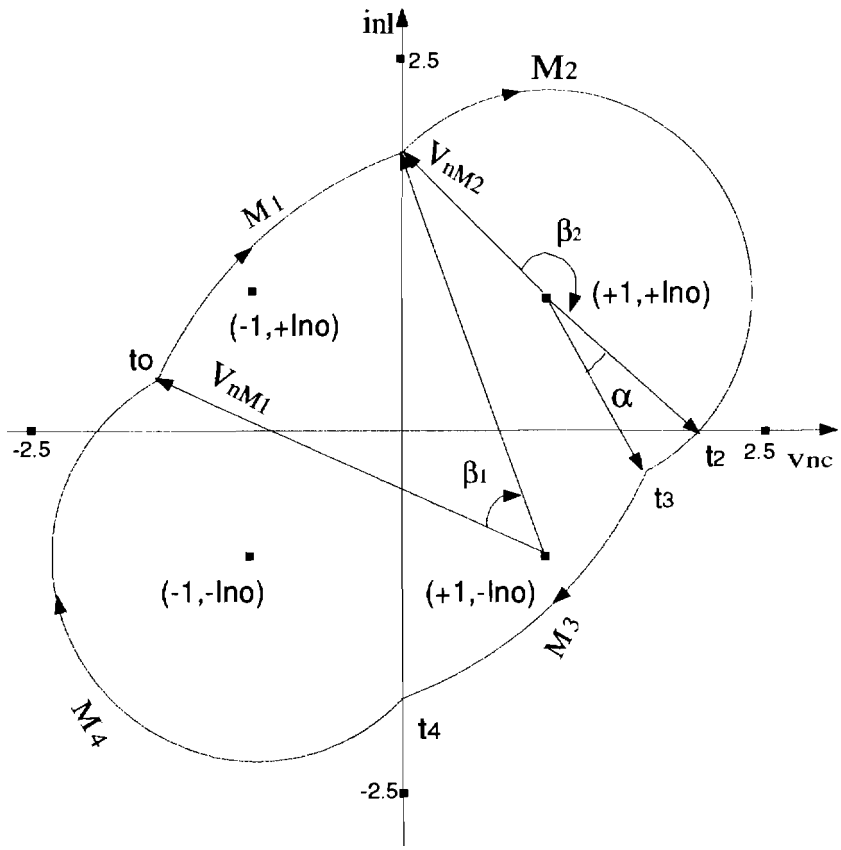

Figure 3.9 PRC state plane diagram for $f_s < f_0$

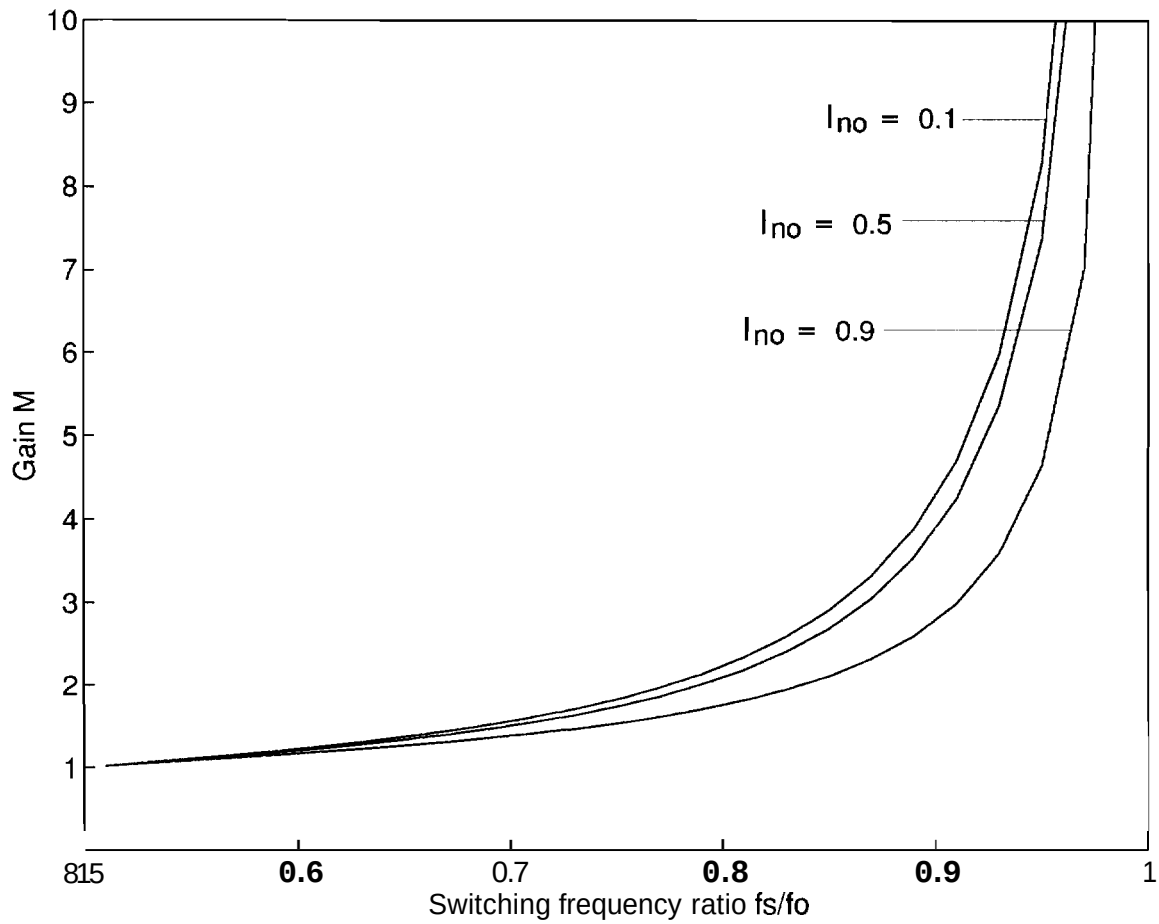

Figure 3.10 PRC control characteristics for $f_s < f_0$

3.4 Comparison of Operation Above and Below Resonance

All the advantages of operating above resonance mentioned in tlie previous chapter are equally applicable for PRC also. Thus in order to reduce tlie losses associated with the turn-off of the power switches, small snubber capacitors can be employed.

At switching frequencies less than $0.5f_0$, the converter operates in the discontinuous conduction mode. Note from Fig. 3.5 that at heavy loads the slope of the characteristics becomes steeper and tlie gain is zero beyond a certain switching frequency. This is actually due to the converter entering a discontinuous mode called the discontinuous capacitor voltage mode and is not analyzed here. In this mode the capacitor voltage remains at zero for a short duration. Thus the gain actually does not become zero at this point, but the converter enters DCM. An expression can be derived for tlie critical value of I_{n0} above which the converter enters discontinuous conduction mode[JE88]. It is given by

$$I_{n0crit} = \sqrt{\sin(\gamma/2)^2 + \sin(\gamma/4)^2} - \sin(\gamma/2)$$

where $\gamma = \pi/f_{sn}$ as defined before.

3.5 Summary

The main advantages of PRC are

1. As seen from Fig. 3.6 it can regulate tlie output at no load.

2. It is naturally short circuit proof. This can be easily seen because even with the resonant capacitor shorted, the current in the circuit is limited by the impedance of the inductor. Hence it is suitable for applications with severe short circuit requirements.

3. Since power is transferred to output by the resonant capacitor voltage, it appears as a voltage source and hence is more suited for multiple outputs. Also since the frequency of operation is rather insensitive lo load variation, good cross-regulation is obtained for multi-output power supplies.

4. They can operate as step up as well as step down converters unlike series resonant converters.

5. It is suitable for low-output-voltage high-output-current applications. This is because high current capacitors are not needed since the output inductor limits the ripple current carried by the output capacitor.

Its main disadvantage is that the current carried by the power switches and resonant components are relatively independent of the load. Thus the light-load efficiency of the converter is poor. This circulating current increases as the input voltage to the converter increases. Hence it is not suitable in applications where the input voltage fluctuates over a wide range and which require it to operate considerably below its design power.

4. SERIES PARALLEL RESONANT CONVERTER

As seen from the previous two chapters, both series resonant converter and parallel resonant converter possess one serious disadvantage. i.e., lack of no-load regulation for SRC and circulating current independent of load for PRC. The series-parallel resonant converter eliminates both these disadvantages while keeping the best characteristics of SRC and PRC'. Fig. 4.1 shows the circuit diagram of a series parallel resonant converter. It is derived by a simple modification to the parallel resonant circuit. i.e., addition of the series capacitor C_s.

Although the converter circuit is a third order system and the state plane analysis for such a converter would be much more complex, it can be shown that by proper transformation of state variables the steady state solution can he derived from a two dimensional state plane analysis [BL89]. This is done by summing up the voltage across the series and parallel resonant capacitors and treating it as a single state. Once this is done, the analysis of this converter closely follows that of the PRC. But for our purposes, which is primarily to derive the control characteristics of the converter, a simpler technique based on classical AC circuit analysis can be employed [Ste88].

4.1 Circuit Analysis

Here we use a straight forward AC analysis to determine the gain of the converter circuit shown in Fig. 1.1. Although we assume that the converter is excited by AC sinusoidal voltages for the analysis, we can account for the actual square wave voltages by treating the AC voltages as their fundamental component. Since the rectifier-filter combination acts as an impedance transformer, the AC resistance will be different

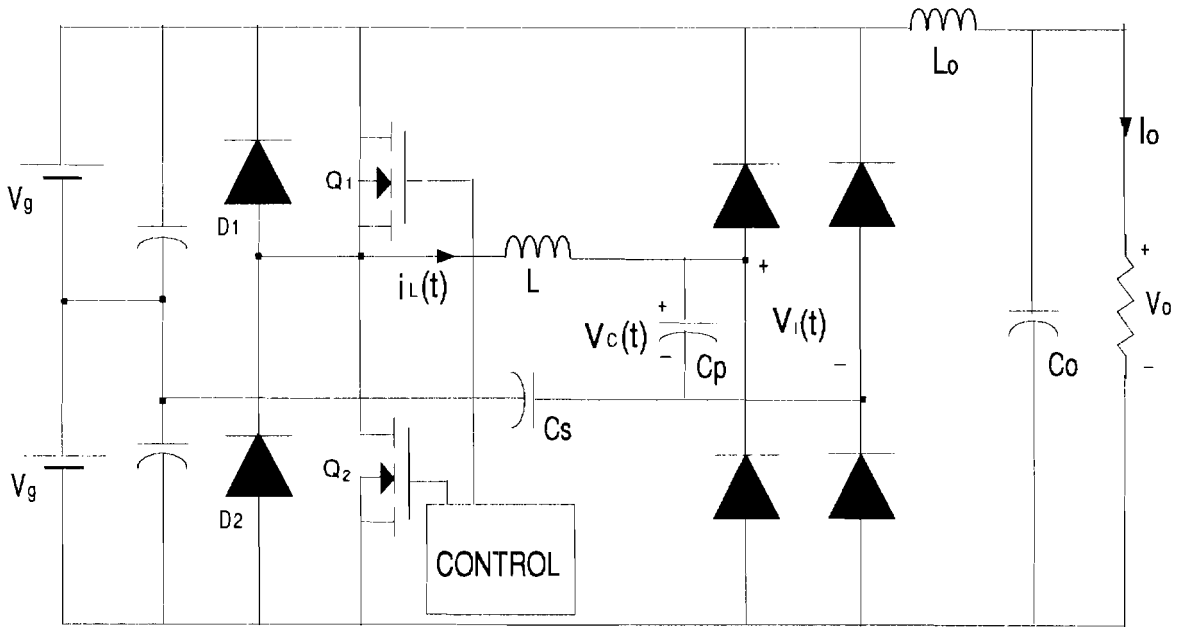

Figure 4.1 Conventional SPRC ciruit diagram

from the load resistance of the converter. Incorporating this, an expression for the gain can be derived from the AC analysis as

$$\frac{V_0}{V_g} = \frac{\frac{C_s}{C_p}}{\frac{\pi^2}{8}\left[1 + \frac{C_s}{C_p} - \left[\frac{f_s}{f_{so}}\right]^2\right] + jQ_s\left[\frac{f_s}{f_{so}} - \frac{f_{so}}{f_s}\right]} \qquad [4.1]$$

where

$$Q_s = \frac{2\pi f_s L}{R_0}$$

$$f_{so} = \frac{1}{\sqrt{LC_s}}$$

where Q_s is the series Q of the circuit,. f_s is the switching frequency and f_{so} is the series resonant frequency. This equation is fairly accurate above resonance where the filtering action of the resonant circuit is sufficient to allow approximate sine waves of current to be in the circuit even though the applied voltage is a square wave. As seen from equation 4.1 the gain depends on the ratio of C_p to C_s and this determines the series or parallel resonant characteristics of the circuit,. In Fig. 4.2 the control characteristics of tlie converter are shown for the case when $C_s = C_p$ and Fig. 4.3 shows them when C, $= 2C_p$. As seen from the characteristics, for Q_s greater than three, the peaks of of the resonant curves appear at approximately the same frequency as the resonant frequency of the series capacitor and series inductance. Thus at these values of Q,, there is almost no effect of the parallel resonant capacitor in the circuit and the converter approaches the characteristics of conventional series resonant converter. Rut as the load on the converter decreases the resonant peak moves higher in frequency. This is because at light load the equivalent resonant capacitance is given by the series combination of C_p and C,. Thus at. light loacls or no load the resonant peak occurs at a frequency given by

$$f_s = \frac{1}{2\pi\sqrt{\frac{LC_pC_s}{C_p+C_s}}} \qquad [4.2]$$

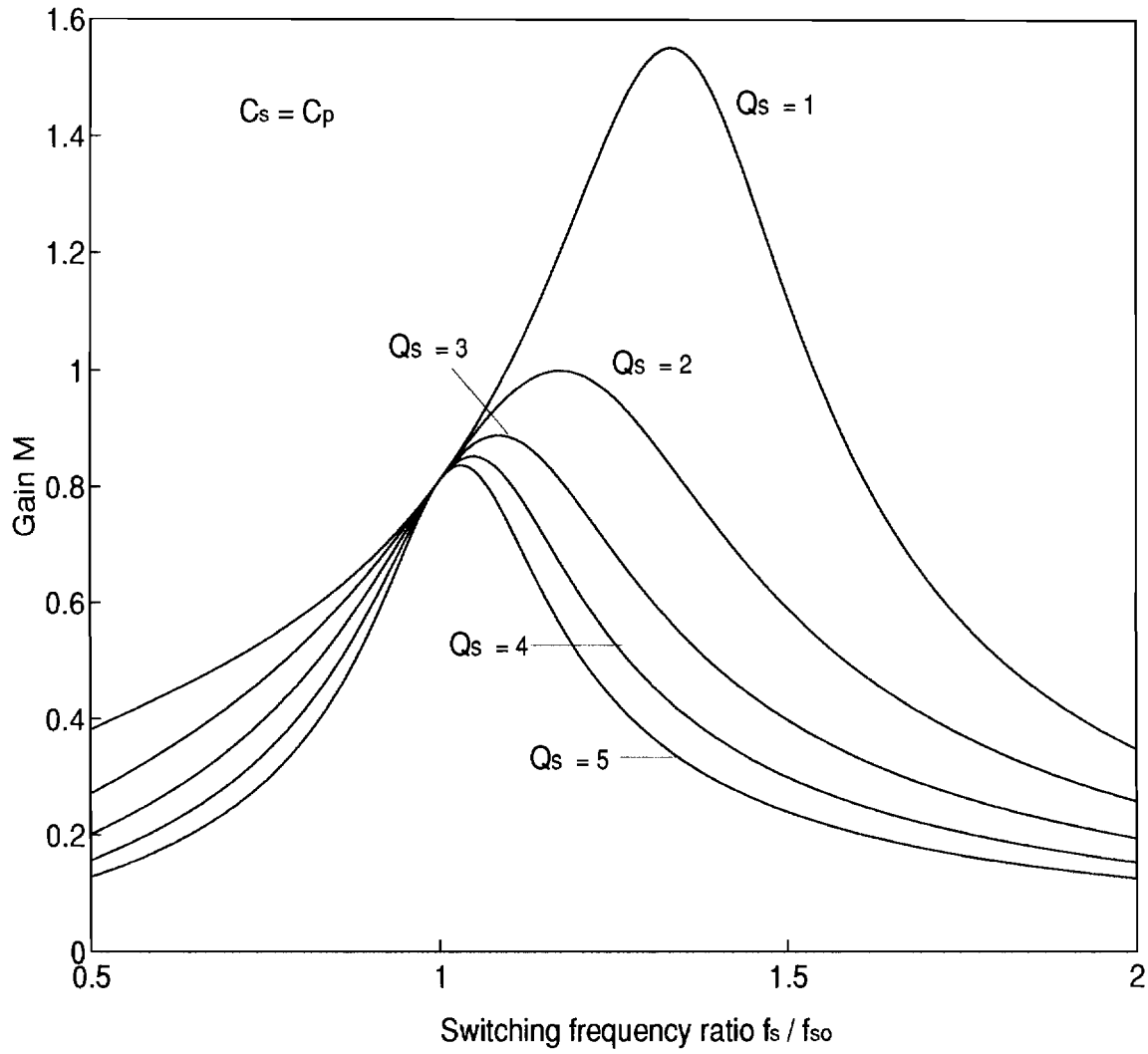

Figure 4.2 Control characteristics when $C_s = C_p$

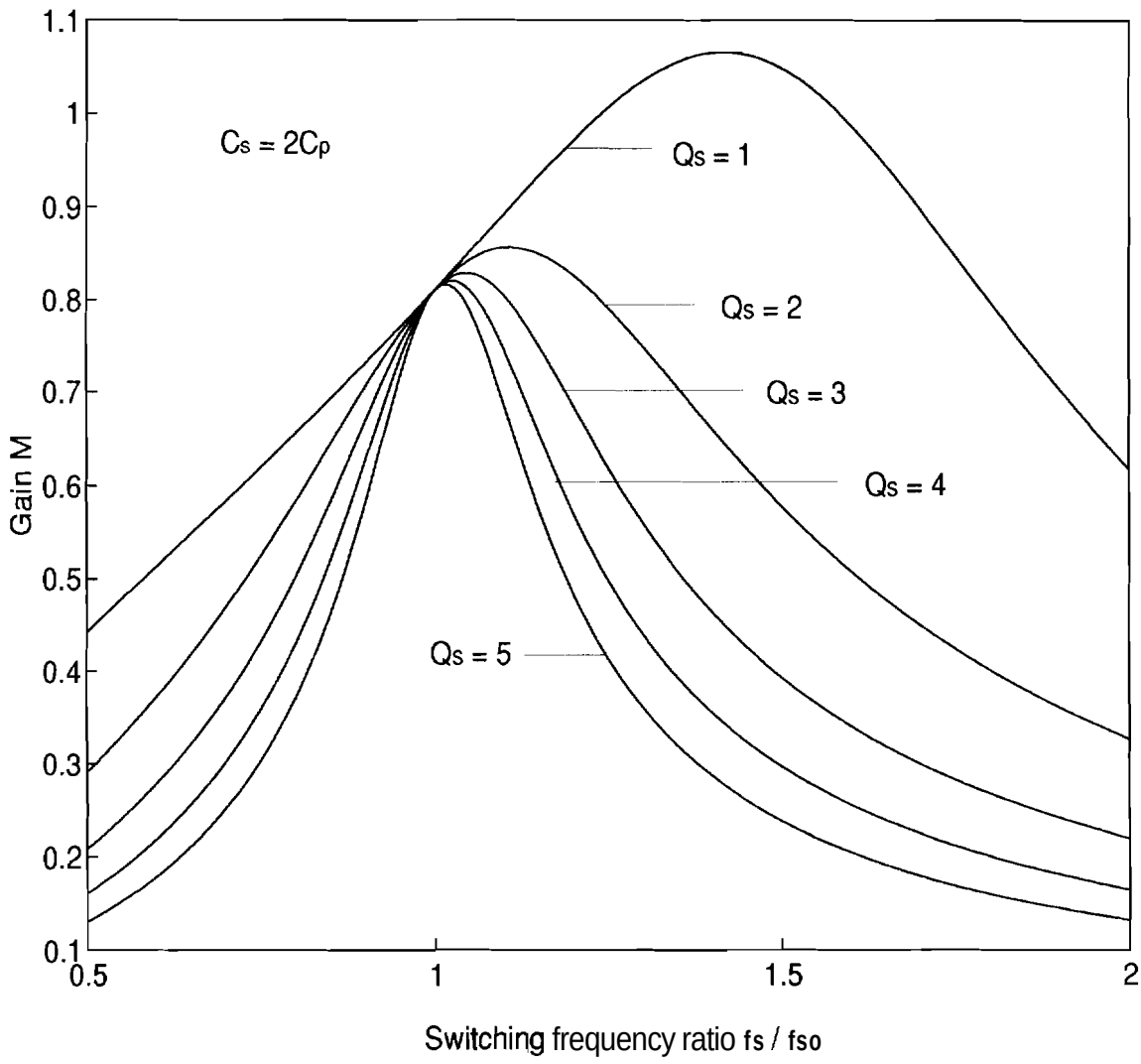

Figure 4.3 Control characteristics when $C_s = 2C_p$

As Q_s decreases Q_p, the Q of the parallel resonant circuit given by the reciprocal of Q_s increases. i.e., as the load decreases the cliaracteristics of the converter move from those of a series-resonant to those of a parallel-resonant.

4.2 Summary

Here the advantages of series parallel resonant converter which makes it more desirable than conventional SHC or PRC will be described.

From the characteristics in Fig. 4.2 it is clear that the converter can operate and regulate voltage at no load provided that the parallel-resonant capacitor C_p is not too small. If C_p is very small tlie converter characteristics revert to those of a series resonant converter. Thus the value of C_p is critical in the sense that it determines the series-resonant or parallel-resonant cliaracteristics of the converter. Also as C_p gets smaller, lesser selectivity is available in the resonant curves. This can be easily seen by comparing figures 4.2 and 4.3. For a constant gain, say 0.5 at a light load of $Q_s = 1$. the frequency of operation when $C_s = 2C_p$ is much higher than for the case of $C_s = C_p$. So as C_p becomes smaller the controller will have to switch through a wider range of frequencies.

Also if the circuit components are properly selected, the input current decreases as the load iucrcascs thereby yielding good part-load efficiency. It is ad antageous lo select the circuit components so that full load Q, is high. Then the converter appears essentially as a series resonant converter and the circulating current will decrease as the load decreases. As the load decreases further the converter takes on the cllaracteristics of a PRC and the circulating current no longer decreases with load.

Thus there is a trade-off in the selection of C_p. While higher values of C_p results in higher circulating current, lower values of C_p makes tlie upper frequency needed at light loads high. In practise, it is found that $C_s = C_p$ is a good design compromise which will result in good part loacl efficiency and operation at no load with reasonable frequency.

4.3 Control of Resonant Converters

Although resonant converters have become quite popular, their control aspects are not well understood as those of PWM converters. In a PWM converter the output energy storage filter usually has a very large time constant compared to the switching period of the converter. The output is regulated by directly controlling the energy input to the slow responding filter. The duty cycle control method adopted to vary the energy input level is simple, straightforward and easy to implement in a feedback controller. On the other hand, in resonant, converters two sets of energy storage elements are present. The output filter with large time constant and resonant circuit with small time constant. The output is controlletl indirectly through the control of resonant tank energy. The tank circuit possesses fast dynamics and exchanges large amount of pulsating energy with the source and the load in each half cycle of a switching period. Because of the presence of the resonant tank circuit with its fast transient response, the control of resonant converters is much more complex than that of its PWM counterparts [OL84b].

4.3.1 Frequency Control

Frequency control is the simplest and most commonly used control method for resonant converters. Since the resonant tank impedance depends on thc frequency of operation, output can be regulated by controlling the switching frequency f_s. The feedback controller determines the switching frequency on a transient basis depending on the error between the reference input and the system output. Most commercially available resonant mode controllers use variable frequency control. It must be noted that although various other control schemes can be employed for these basic topologies [OL84b], because of the inherent characteristics of resonant circuit, all these control methods effectively employ some sort of frequency modulation. The transient response of frequency modulation control is rather poor. This can be seen from Fig. *r2.4* where a step change in the load condition is simulated. Tlie system takes

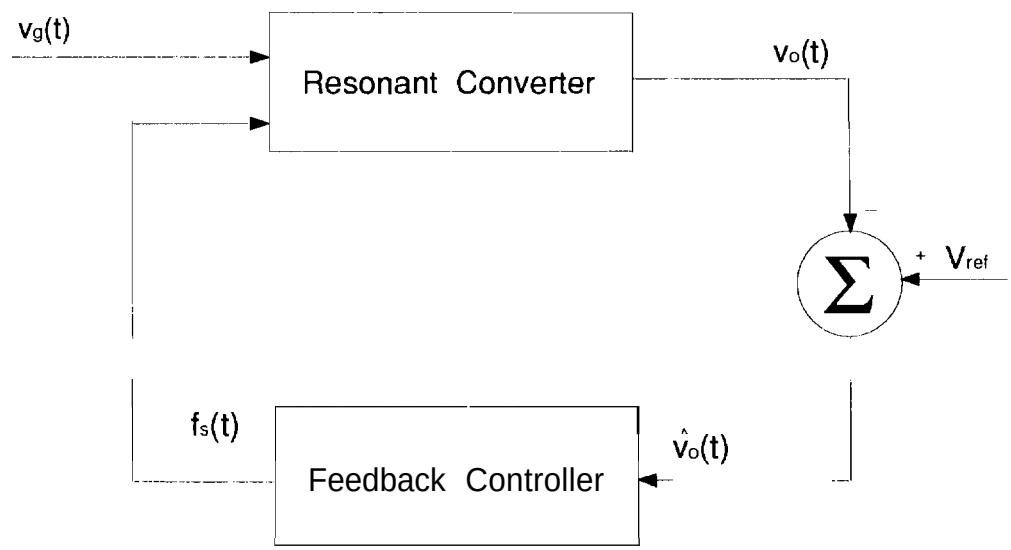

Figure 4.4 Resonant converter with feedback control

several cycles to attain a new steady state. A control technique that drastically improves the transient response is the resonant tank control [OH93]. Here the control law is expressed as a linear combination of the capacitor voltage and incluctor current. When this sum reaches a value transiently updated by the control. the switches ate turned off. But variable frequency control in general has certain disadvantages. It is difficult to design suitable EMI filters when the switching frequency is varying continuously. Also the magnetic components in the converter cannot be effectively utilized under this type of operation. There are several topologies which achieve constant frequency operation with some modifications to the basic circuit. Two such converters are discussed below.

1.3.2 Phase Controlled converters

In these converters, most of which are of the full-bridge type, two identical half-bridge converters share the same load. The DC output voltage is regulated by varying the phase shift between the voltages driving the two half-bridges while maintaining a constant switching frequency. The disadvantages with this type of converter are that higher number of resonant components and switches are needed. The method of control is also more complex. It is import ant to have both resonant circuits identical. If not, there will be an imbalance in the amplitude of currents in the two half bridges which will lead to unstable operation[CK93].

4.3.3 Capacitor Voltage Clamped converters

In this type of converters, during the course of one switching period there are short durations during which the capacitor voltage is clamped at a certain value. By varying the duration of this clamping, the output voltage can be regulated. Also because of this clamping, the converter has lesser stress appearing on the circuit components. The drawback with this method is that analysis as well as control is more complex and that a higher number of switching devices are needed. This method is usually used with series resonant converters.

5. CONCLUSIONS

5.1 Observations

Our objective was to study the basic configurations of resonant converters and to compare their performance when opcratcd under different conditions. Jt was found that the analysis of resonant converters is much more involved than that of PWM converters. This is because in resonant converters the energy transfer from input to output involves two sets of energy storage elements, the resonanl filter and the output filter. Often tlie anomalous sequences of conduction exhibited by practical systcrns are difficult to explain by time-domain methods of analysis.

The state plane method was used as the basic analysis tool because of its advantages over other methods. First of all it gives a better insight of the operation of the converter. Based on the state plane diagram all the converter characteristics can be derived. For any resonant mode converter the state plane trajectory consists of only circular arcs arid straight lines. Since the state plane clearly portrays the steady state as well as transient operation of the converter, it is a powerful tool for design purposes.

From analytical and simulation results it is found that operating above the resonant frequency is the favorable range of operation for resonant converters. In this range of operation the switching losses are kept to a minimum, diodes are not required to have very good reverse recovery characteristics and there is more effective use of the magnetic components within the converter. These features directly contrast with operation below resonance. Also the stresses appearing across the circuit components are lower when operated above resonance. These results had also been verified experimentally.

5.2 Recommendations

Both the serics resonant converter and parallel resonant converter are commercially used in switching power supplies nowadays. But, because of the disadvantages discussed before, they are not suitable for some applications. Hence hybrid topologies like series parallel resonant converters are attaining more attention. There are several variations of SPRC discussed in the literature either with more reactive components or switches and yielding a marginal improvement in performance. Ideally we would like these types of high efficiency converters to be able to regulate their output at constant switching frequency. But, up to this point efforts in this area has resulted only in converters with a large number of switches and other reactive components and usually with a limitation on the range of the output load. Thus their efficiency is significantly less than that of the conventional topologies and are less reliable.

BIBLIOGRAPHY

BIBLIOGRAPHY

[Bha92] A.K.S. Bhat. Analysis and design of series-parallel resonant power supply. *IEEE Trans. on Aerospace and Electronic ,Systems,*28(1):249–258, January 1992.

[BL89] I. Batarseh and C.Q. Lee. High-frequency high-order parallel resonant converter. *IEEE Trans. on Industrial Electronics,* 36(4):485–498, November 1989.

[Bro90] M. Brown. *Practical Switching Power Supply Design.* Academic Press Inc., 1990.

[BS90] A.K.S. Bhat and M.M. Swamy. Analysis and design of parallel resonant converter including the effect of a high frequency transformer. *IEEE Trans. on Industrial Electronics*, 37(4):297–306, August 1990.

[Chr89] G.C. Chryssis. *High Frequency Switching Power Supplies.* McGraw-Hill, 1989.

[CK93] D. Czarkowski and M.K. Kazimierczkuk. Phase-controlled series-parallel resonant converter. *IEEE Trans. on Power Electronics*, 8(3):265–274, July 1993.

[JE88] S.D. Johnson and W. Erickson, R. Steady-state analysis and design of the parallel resonant converter. *IEEE Trans. on Power Electronics,* 3(1):93–103, January 1988.

[KSV91] J.G. Kassakian, M.F. Schlecht, and G.C. Verghese. *Principles of Power Electronics*, chapter 9. Addison-Wesley, 1991.

[KW92] M.K. Kazimierczuk and S. Wang. Frequency-domain analysis for series resonant converter for continous conduction mode. *IEEE Trans. on Power Electronics*, 7(2):270–279, April 1992.

[LBLU88] C.Q. Lee, I. Batarseh, R. Liu, and A. Upadhyay. Comparison of capacitive and inductive coupled parallel resonant convertes. In *IEEE-APEC-88,* pages 157 166, 1988.

[LBR88] C.Q. Lee, I. Batarseh, and Liu R. Design of capacitively coupled lcc-type parallel resonant converter. In *IECON' 88*, pages 157-166, *1988*.

[LK86] C.Q. Lee and Siri K. Analysis and design of series resonant converter by state plane diagram. *IEEE Trans. on Aerospace and Electronic Systems*, 22:757 763, November *1986*.

[MC76] R.D. Middlebrook and S. Cuk. A general unified approach to modelling switching converter power stages. In *IEEE Power Electronics Specialists Conference*, pages 824 848, 1976.

[Mor92] S. Morrison. Analysis of a hybrid series-parallel resonant bridge converter. *IEEE Trans. on Power Electronics*, 7(1):119–127, January *1992*.

[MUR89] N. Mohan, T.M. Undeland, and W.P. Robbins. *Power Electronics*, chapter 7. John Wiley and Sons, 1989.

[OH93] R. Oruganti and T.C. How. Resonant-tank control of parallel resonant converter. *IEEE Trans. on Power Electronics*, 8(2):127–133, April *1993*.

[OL84a] R. Oruganti and F.C. Lee. Resonant power processors: Part i - state plane analysis. In *IEEE-IAS-1984 Annual Meeting Conference*, pages 868–878, *1984*.

[OL84b] R. Oruganti and F.C. Lee. Resonant power processors part ii - methods of control. In *IEEE-IAS-1984 Annual Meeting Conference*, pages 868–878, 1984.

[Sev92] R.P. Severns. Topologies for three-element resonant converters. *IEEE Trails. on Power Electronics*, 7(1):89–97, January *1992*.

[SL92] S. Sooksatra and C.Q. Lee. Pwm controlled src with inductive output filter at constant switching frequency. *IEEE Trans. on Power Electronics*, 7(2):289 291, April *1992*.

[SRH92] M.J. Schutten, Steigerwald R.L., and Kheraluwala H. Characteristics of load resonant converters operated in a high power factor mode. *IEEE Trans. on Power Electronics*, 7(2):304–314, April *1992*.

[Ste88] R.L. Steigerwald. A comparison of half-bridge resonant converter topologies. *IEEE Trans. on Power Electronics*, 3(2):174-182, April *1988*.

[VC83] V. Vorperian and S. Cuk. Small signal analysis of resonant converters. In *IEEE Power Electronics Specialists Conference*, pages *265–278, 1983*.

APPENDIX

APPENDIX
SIMUCATION AND EXPERIMENTAL RESIJLTS

A.1 Series Resonant Converter

A prototype series resonant converter was built to verify the characteristics and the analytical results obtained. The details of the design are given below. Fig. A.1 shows the complete layout of the power supply. The unit was laid out on a 6in x 4in PCB. By using a ground plane, very good waveforms were obtained with little or no noise at all.

The specifications of the supply are

Main input DC supply	$2V_g$	=	28V – 32V
Load current	I_0	=	0.2A – 0.9A
Output voltage	V_0	=	1101'
Converter resonant frequency	f_0	=	50 khz
Maximum output Power	P_0	=	100W

The following design information was obtained from 2.2.4

Resonant Inductor L	=	10.3 μH
Resonant Capacitor C	=	0.94 μF
Resonant frequency f_0	=	51.15khz
Characteristic Impedance Z_0	=	3.5 Ω
Transformer turns ratio n	=	$\frac{1}{9}$

Since we chose Q as 2.25, we can find the AC resistance as

$$R_{ac} = \frac{Z_0}{Q} = 1.55\,\Omega$$

Hence the DC load resistance will be

$$R_L = \frac{\pi^2}{8} R_{ac} \frac{1}{n}^2 \approx 155\,\Omega$$

A 100W lamp was used as the load for the supply.

Since the leakage inductance of the primary winding of the transformer is 0.3μ H, the effective value of the inductance required off the resonant inductor is 10μ H. Then the number of turns needed is given by the equation

$$\begin{aligned} N &= 1000\sqrt{\frac{L_{mH}}{A_L}} \\ &= 6 \text{ turns} \end{aligned}$$

where A_L is a constant of the core. Here a 3C8 core with an A_L of 275 was used.

An MC 7812 voltage regulator is used to supply power to the controller IC.

The commanded switching frequency from the controller is programmed to be locked between 51khz and 78khz. This is done by proper selection of the components for the controller. A deadtime of 0.5μs is chosen between the gate drives to the two switches. The components in the controller section are calculated using the equations given in the data sheet of the IC. An optoisolator 4N35 is used for isolating the output section from the Controller. All the magnetic and semiconductor components used are labeled in Fig. A.1.

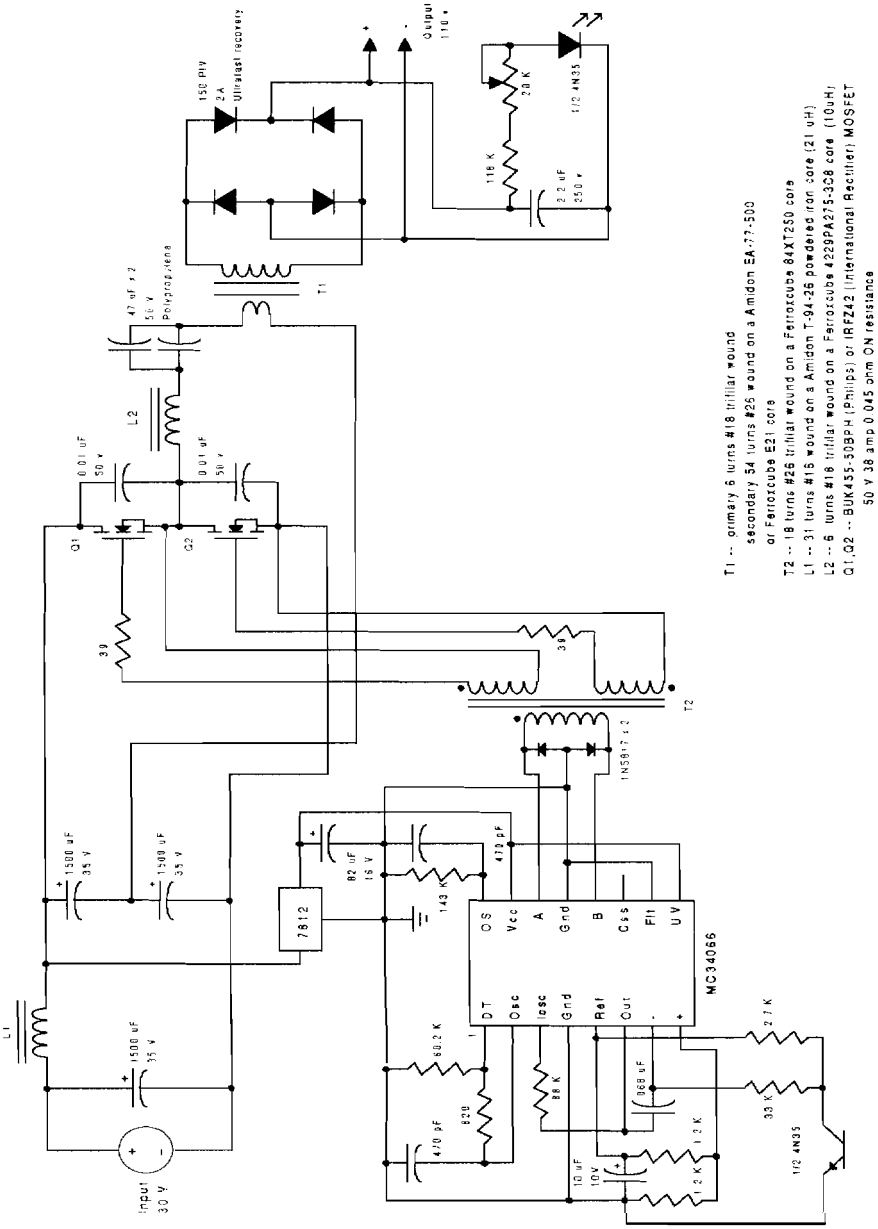

Figure A.1 Circuit layout of fabricated series resonant converter

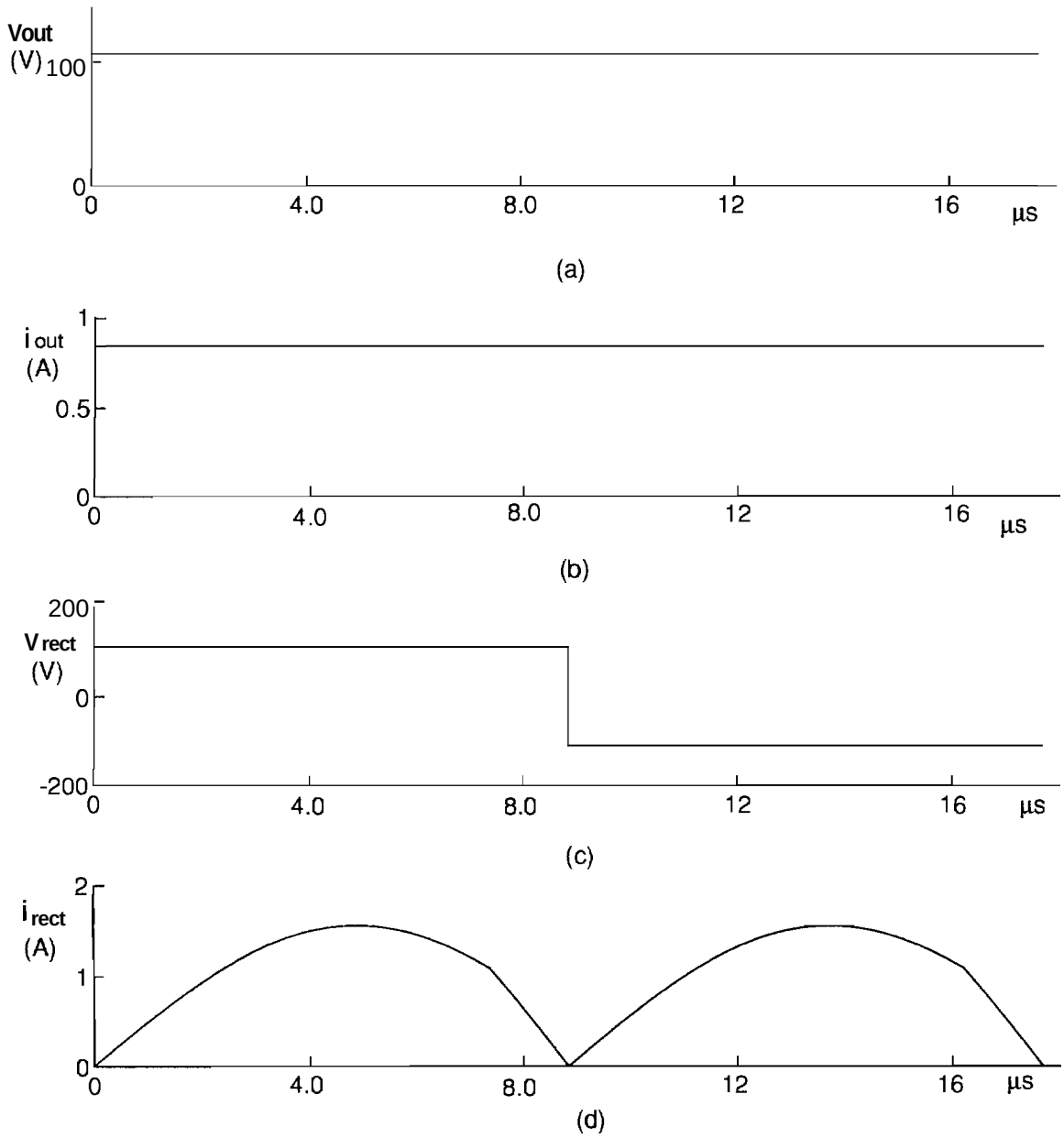

Figure A.2 SRC simulation: rectifier's input and output voltage and current

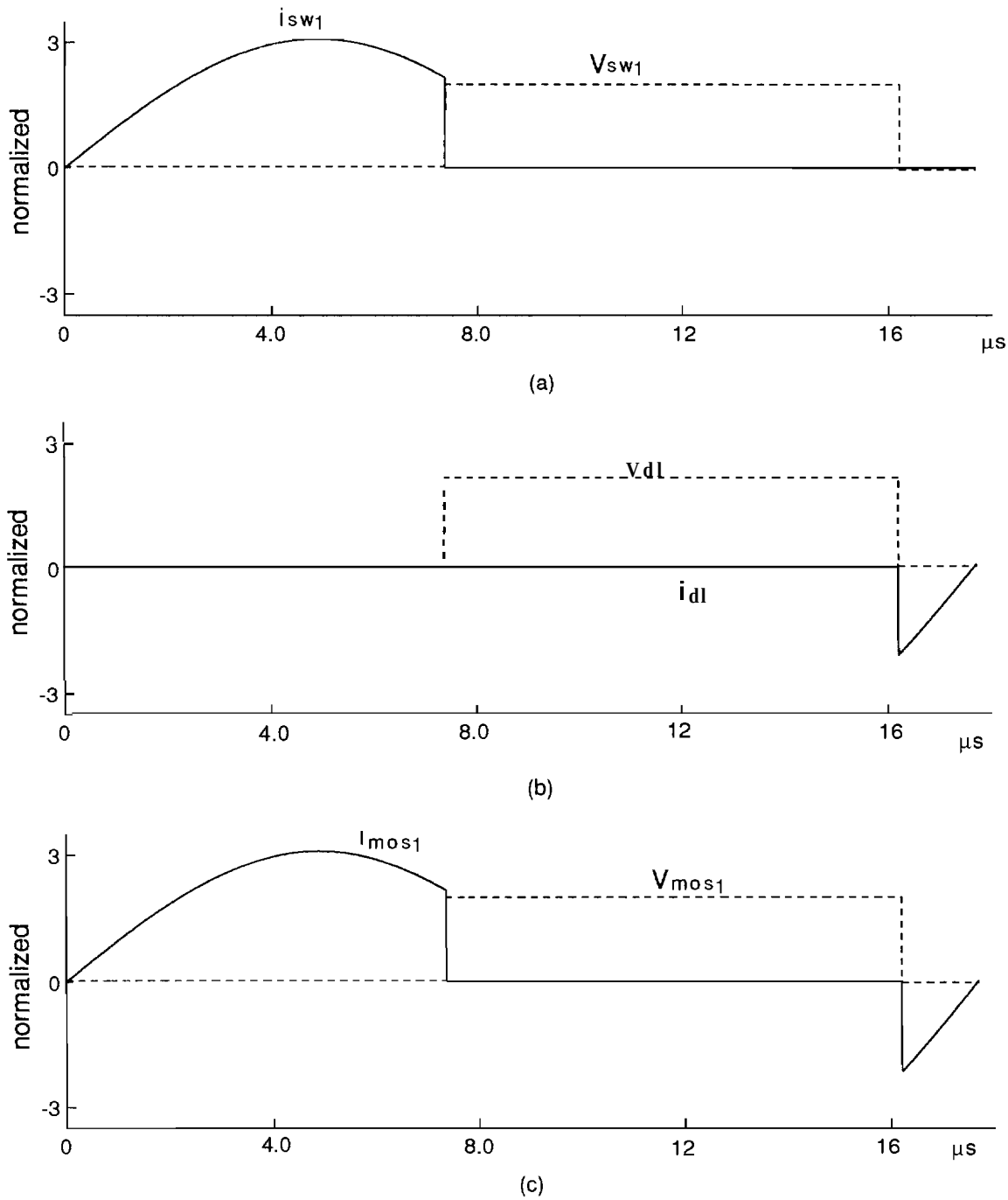

Figure **A.3** SRC simulation: switch voltage and current

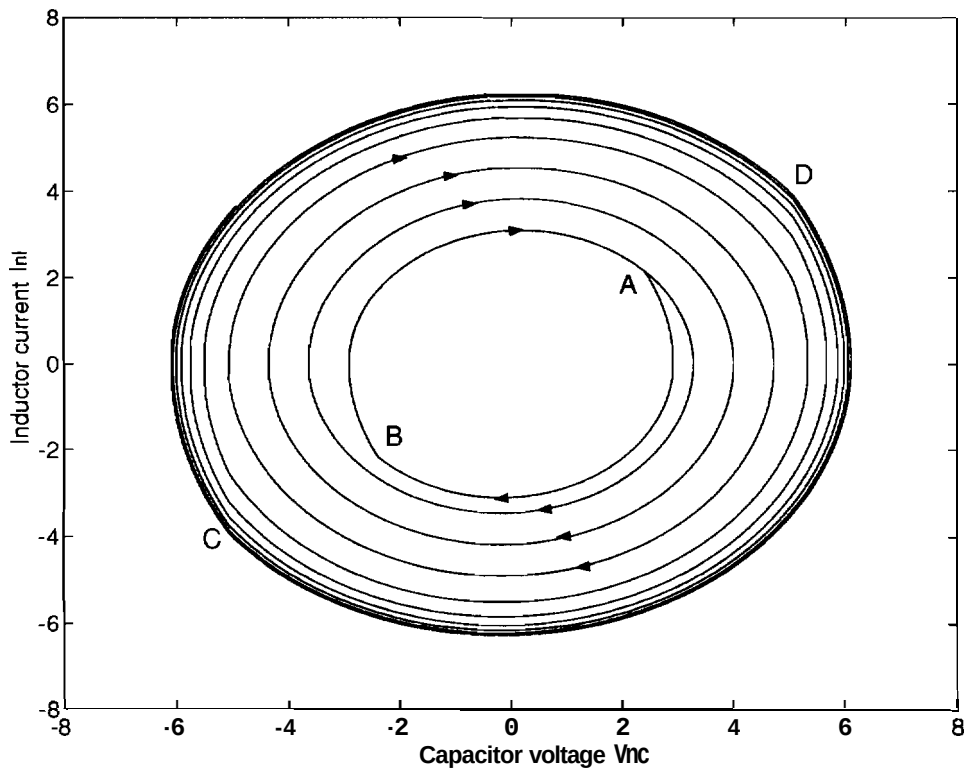

Figure A.4 SRC simulation: step change in load on the state plane

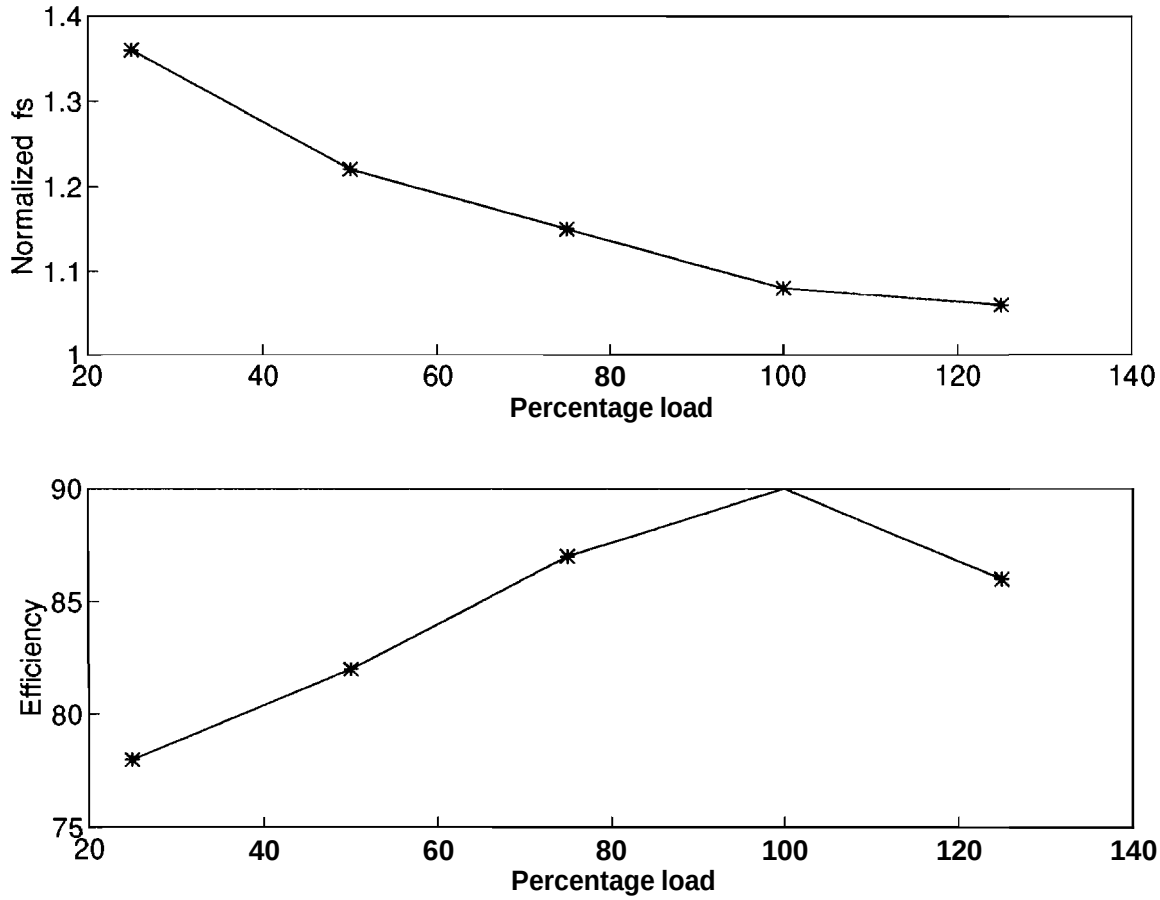

Figure A.5 SRC: measured efficiency and switching frequency

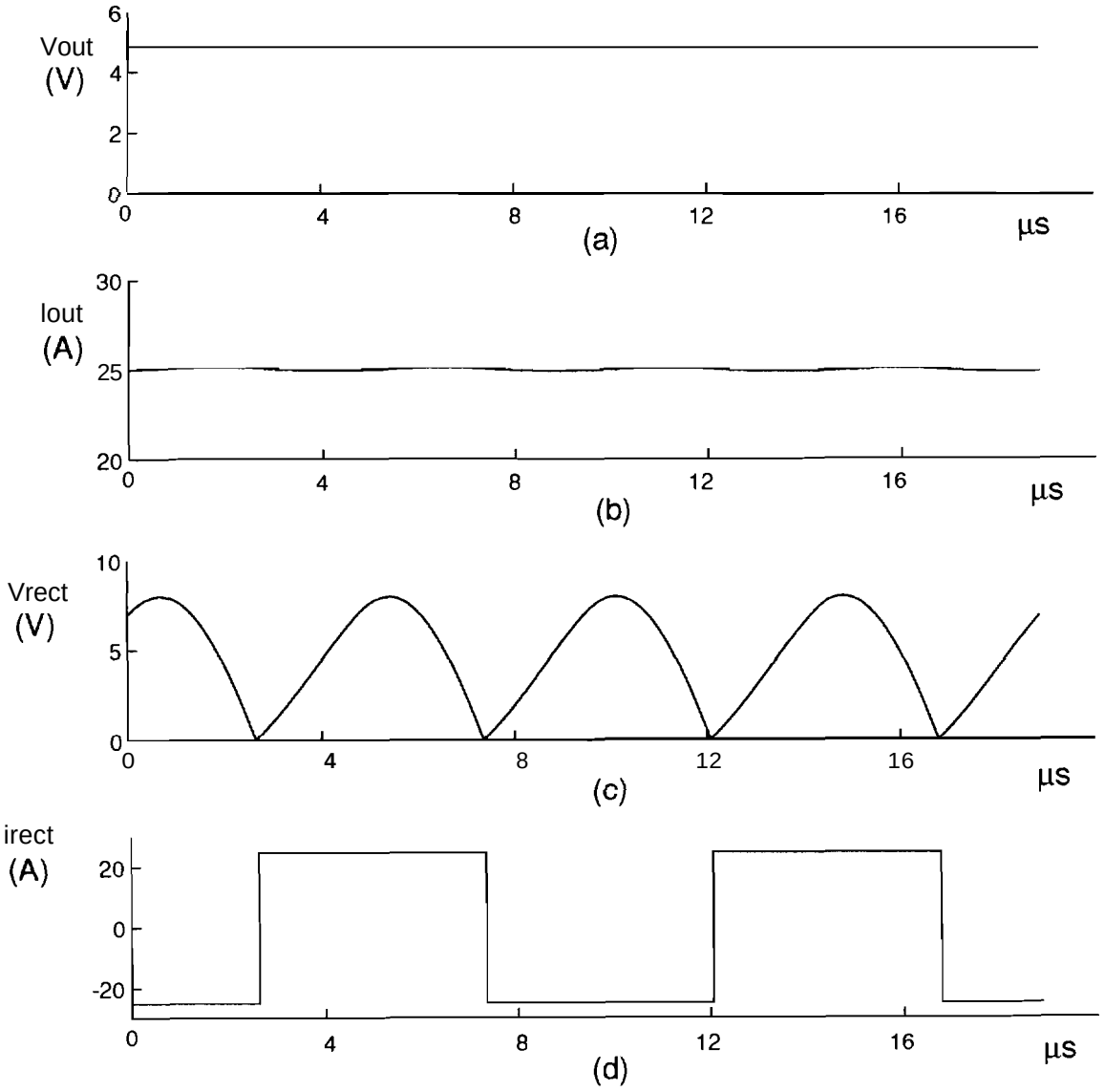

Figure A.6 PRC simulation: rectifier's input and output voltage and current

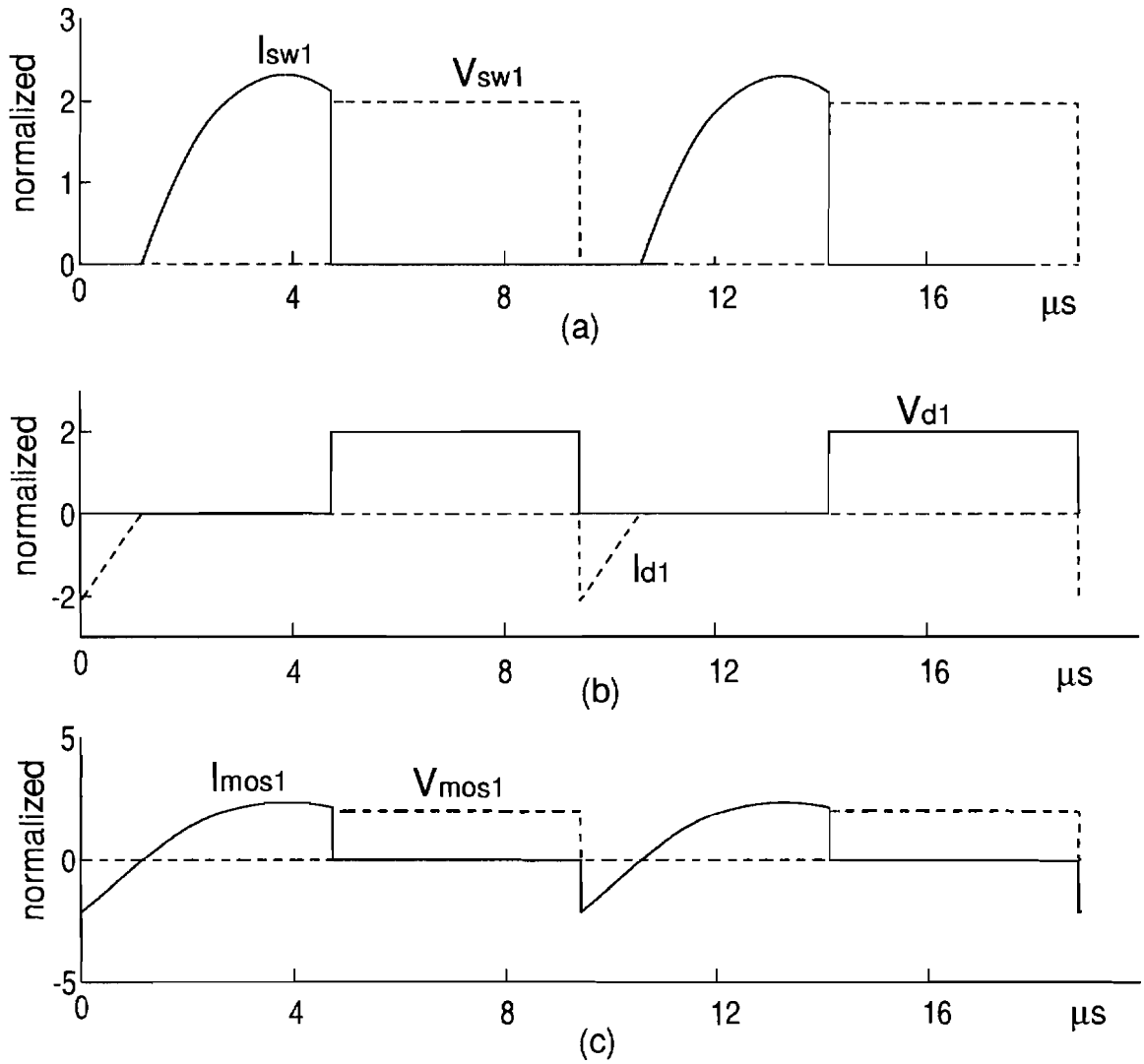

Figure A.7 PRC simulation: switch voltage and current

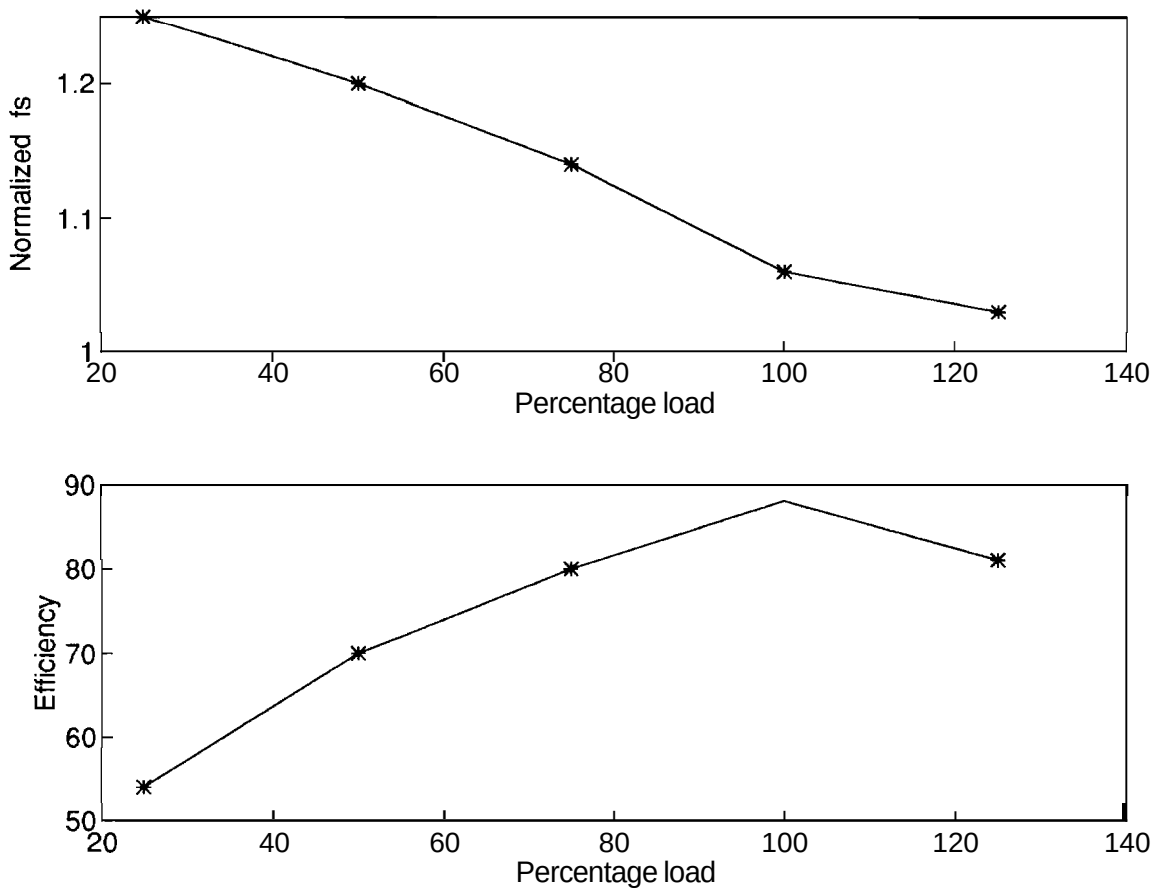

Figure A.8 PRC: measured efficiency and switching frequency